198
8/6/79

Ls. 2971

LA-7862-MS
Informal Report

Experiments on the ZT-S Reversed-Field Pinch

August—December 1978

University of California

LOS ALAMOS SCIENTIFIC LABORATORY
Post Office Box 1663 Los Alamos, New Mexico 87545

LA-7862-MS
Informal Report
UC-20f
Issued: June 1979

Experiments on the ZT-S Reversed-Field Pinch

August—December 1978

A. R. Jacobson

EXPERIMENTS ON THE ZT-S REVERSED-FIELD PINCH, AUGUST-DECEMBER 1978

by

A. R. Jacobson

ABSTRACT

During the latter half of 1978 the ZT-S reversed-field pinch was used to explore the utility of pitch-programming techniques in setting up stable diffuse pinch profiles. Several experimental observations relating to this goal are presented.

I. INTRODUCTION

This report describes a series of experiments performed by the author in collaboration with L. C. Burkhardt. The primary motivation was to explore a new method of achieving reversed-field pinch (RFP) equilibria. The results are inconclusive, mainly due to inadequacies in the experimental realization of the desired magnetic field waveforms.

The experiments described below were performed on ZT-S, a small (R/a = 40 cm/7.7 cm) toroidal pinch. An upgraded (greaseless O-ring seals) ceramic torus, for which A. Haberstich was primarily responsible, coupled with an improved oil-free pumping system (due to R. B. Howell), were used. Unfortunately, due to a persistent leak in the torus, the base pressure never was better than 2×10^{-6} torr, far above the outgassing limit. The single pumping port (through a two-inch diameter hole in the primary) was equipped with an undersize metal plug that could be inserted prior to the discharge, in order to reduce the magnetic field errors associated with the hole. Surprisingly, running ZT-S with or without the plug seemed to make no difference.

II. PITCH-PROGRAMMING EXPERIMENTS

A. Inadequacies of the Experiments

One possible approach to the formation of RFP equilibria is the technique of pitch programming.[1] The method has been usefully applied on the SPICA screw-pinch experiment[2] and has been proposed[3] for reversed-field pinches at Los Alamos. Computer simulations[4] of pitch programming on the ZT-S reversed-field pinch experiment have indicated that pitch programming may indeed be effective in this apparatus. The computer runs considered the following case: poloidal field (at wall) rising to a peak in 4 μs; toroidal field (at wall) ringing through three-quarters of a period and reaching a negative peak at 4 μs. Both field components are fired together, and are crowbarred together at 4 μs. They are shown in Fig. 1a.

The actual field waveforms obtained on the ZT-S experiment have not provided a satisfactory approximation of the prescription in Fig. 1a. Several experimental waveforms have been tried, and in each case there is only a partial resemblance to the idealized time histories of the fields. There are four basic reasons for the discrepancies between ideal and actual waveforms:

1) Whereas the ideal case has little or no bias toroidal field, the experiment needs to operate with enough bias field to stabilize the pre-ionization discharge.
2) Strong plasma-circuit coupling causes the toroidal field to rise very sharply at first.
3) Plasma-circuit coupling also causes the reversal level of the toroidal field to be smaller than would be expected on the basis of a vacuum shot.
4) The ZT-S toroidal field coils had a three-quarter period of 9 μs in this experiment, as opposed to the 4 μs ideal case.

One example of an experimental waveform is shown in Fig. 1b. Note the offset time scale, so that t_o is at 56 μs on the abscissa. An attempt was made to arrive at crowbarred fields whose values at the wall would correspond to the ideal case of Fig. 1a. The tradeoff entailed using a larger initial rise in the toroidal field than was considered in the computer model. This was necessitated by plasma-circuit coupling, which (as mentioned above) causes the reversed crowbarred toroidal field at the wall to be weaker than expected on the basis of a vacuum shot. The ratio of the fields at the end of the graph (t = 64 μs) are indeed "correct;" however, the transient phase between

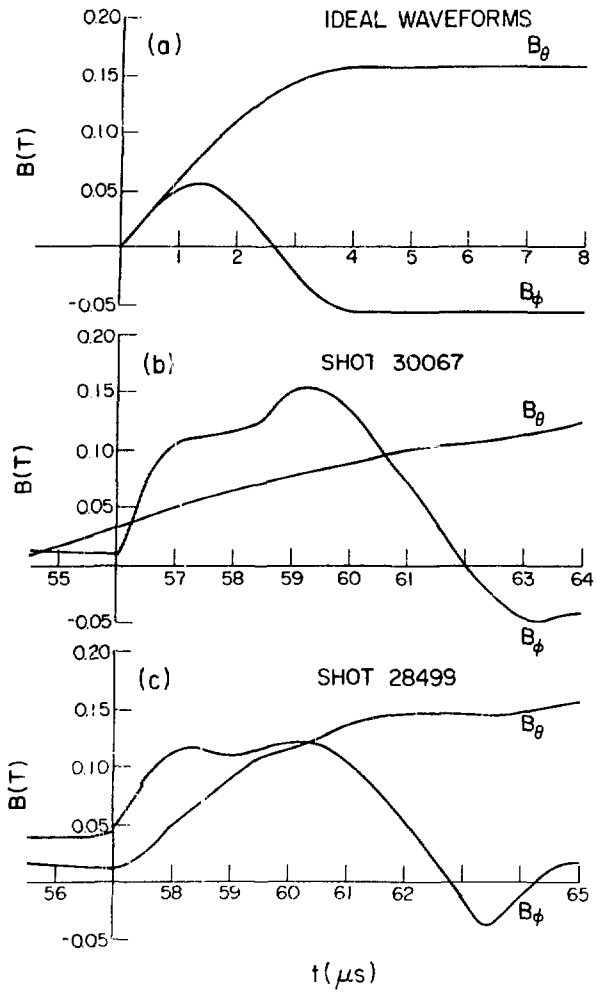

Fig. 1. Waveforms of the toroidal (B_ϕ) and poloidal (B_θ)magnetic fields. Time scales are equal but offset, to allow for preionization.
(a) Ideal case, for which calculations indicate favorable pitch profiles are programmed into the plasma.
(b) Actual case, with high inductance B_θ primary.
(c) Actual case, with low-inductance B_θ primary.

57 and 61 μs does not resemble the ideal case, the toroidal field being much too strong. The dynamics of such shots will be discussed later.

Another set of experimental waveforms is shown in Fig. 1c. The B_θ circuit inductance is less than in shot 30067, so that the poloidal field rises faster. As a result, the time derivatives of the two field components are more nearly equal during the first rise, in common with the ideal case (Fig. 1a). However, the toroidal field reversal is only transient, and the crowbarred toroidal field is actually positive. In addition, substantial bias toroidal field is used (in Fig. 1c) to stabilize the pre-ionization discharge.

B. Early-time Dynamics of Two Types of Pitch-Programming Discharges

The example shot of Fig. 1b (number 30067) is typical of an extensive series of discharges taken under the same conditions. As mentioned above, an excessive initial rise of the toroidal field was necessary to arrive at crowbarred conditions resembling the pitch-programming recipe. This excessive initial toroidal field rise, followed by its rapid removal during programmed reversal, had a catastrophic effect on the plasma confinement. Essentially, the rapid rise of B_ϕ led to a θ-pinch in the plasma interior, with B_θ excluded (by pressure balance) and remaining out near the insulating wall. The poloidal field is shown in Fig. 2a, as a function of both minor radius and

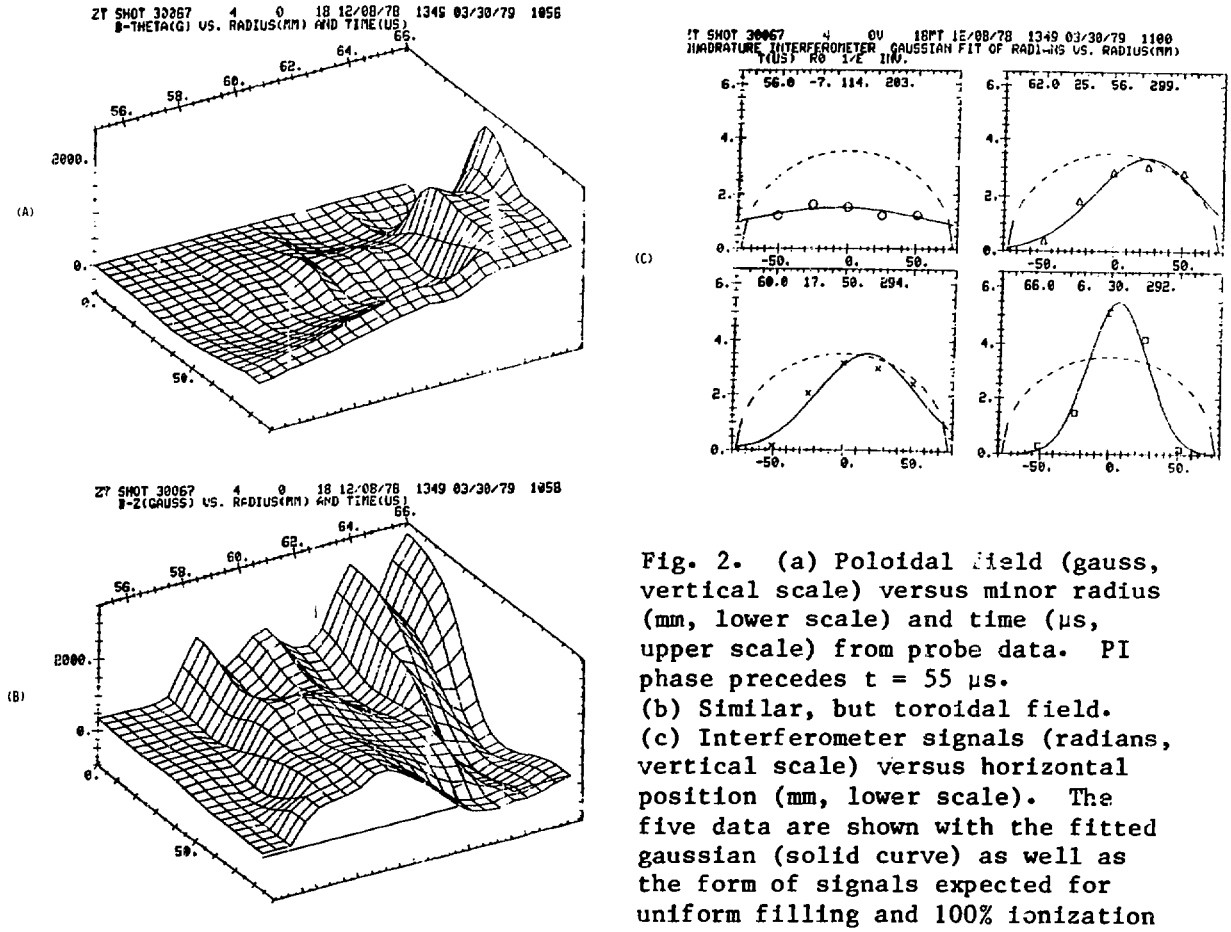

Fig. 2. (a) Poloidal field (gauss, vertical scale) versus minor radius (mm, lower scale) and time (μs, upper scale) from probe data. PI phase precedes t = 55 μs.
(b) Similar, but toroidal field.
(c) Interferometer signals (radians, vertical scale) versus horizontal position (mm, lower scale). The five data are shown with the fitted gaussian (solid curve) as well as the form of signals expected for uniform filling and 100% ionization (dashed curve).

time, during the setup phase. The poloidal field does not penetrate much inside the insulating wall (r = 77 mm) until the toroidal field is reversed, at which time the plasma equilibrium essentially transforms from being θ-pinch-like to being z-pinch-like. This can be seen in Fig. 2b, which shows the toroidal field, in the same format. B_ϕ rushes in at first, and only as it swings back toward zero (at the wall) can B_θ penetrate. At the end of the trace (64-66 μs) the toroidal field is peaked on axis and confined by the poloidal field; the interface appears remarkably sharp.

An unfortunate consequence of the early-time θ-pinch-like equilibrium is a prolonged, close contact between the plasma and the wall. From Fig. 2a, it can be inferred that j_ϕ is virtually on the insulator until the poloidal field is allowed to penetrate the plasma bulk. Likewise, a very large outward toroidal shift is observed as is expected for a toroidal θ-pinch. This can be seen from the multichord interferometer[5] data of Fig. 2c. Pictured in each box are the five chordal phase shifts for each of four times. At each time a gaussian is least-square fitted to the chordal data. The dashed cosine curve is the locus of data that would be expected if the 18 mtorr D_2 gas fill were fully ionized and uniformly distributed in minor radius. The upper left box shows conditions immediately prior to t_o, i.e., at the end of the pre-ionization discharge. The distribution corresponds to uniform density with 48% ionization. The second (lower left) and third (upper right) boxes show the growth and saturation of the outward toroidal shift due to the θ-pinch nature of the equilibrium. In the last box, following the transition to a z-pinch-like equilibrium (with B_ϕ peaked on axis), the plasma column has once again become centered in the major radius direction. A corollary observation based on Fig. 2c is the constancy of the ionization fraction (relative to the 18 mtorr gas fill) between the second and fourth frames. Over a period of 6 μs, the ionization remains conserved at approximately 69%.

The example shot of Fig. 1c (number 28499) is also typical of an extensive series of discharges taken under similar conditions. In this case, the poloidal field rises sufficiently fast that it penetrates the column along with the toroidal field. This early penetration is shown in Fig. 3a. The toroidal field peaks on axis and undergoes m = 0 oscillations against the confining poloidal field, as seen in Fig. 3b. As a result, there is no violent transition (when B_ϕ at the wall is programmed down through zero) from a θ-pinch- to a z-pinch-like equilibrium. Also, as expected, the toroidal

shift is very small compared to the previous example shot. This is apparent from Fig. 3c. In further contrast to shot 30067, the fractional ionization is constantly growing in Fig. 3c, reaching 92% in the last frame.

Thus, by reducing the inductance of the poloidal field circuit, the poloidal field penetration was made adequate for a "stiff" toroidal equilibrium. However, the tendency of the crowbarred toroidal field to become positive worsened, and a true reversed field pinch was not obtained.

C. Observed Particle Containment in Pitch Programming Discharges

Containment of plasma is the sine qua non of CTR toroidal devices. It is a prerequisite for the attainment of long energy replacement times. Measurements of plasma density profiles are routinely made on ZT-S using a multi-chord interferometer[5] illuminated in the infrared. The instrument records the line integral of the electron density along each of five chords, which are normal to the major radius. Even without Abel inversion, one immediately obtains the line density (typically to within five, or at worst ten, percent) as well as the location of the plasma centroid in the major radius direction.

The series of pitch-programming discharges exemplified in Fig. 1b showed poor plasma containment. This is not surprising, considering the difficulties in programming the magnetic fields, as mentioned above. In Fig. 4 are shown some of the interferometer data for shot 30067.

The upper half is analogous to a streak picture. The outer lines are the 1/e loci of the gaussian that is used to fit the phase shifts along five chords. The inner line is the displacement (along major radius) of that gaussian. (Upwards in the ordinate corresponds to outwards in major radius.) The ceramic walls are located at ± 77 (mm) on the ordinate. Where a 1/e locus lies outside the ± 77 (mm) points, this does not mean that plasma extends beyond the wall, but only that the gaussian fit's 1/e location is outside the ceramic-vacuum interface. The lower half of Fig. 4 graphs the line density on the same time scale as the upper half. In the units employed by the data analysis program, the horizontal dashed line corresponds to 100% ionization of the gas fill (18 mtorr D_2). The interruption on the upper half (and straight-line interpolation on the lower half) of Fig. 4 are due to negative curvature of the fitted gaussian.

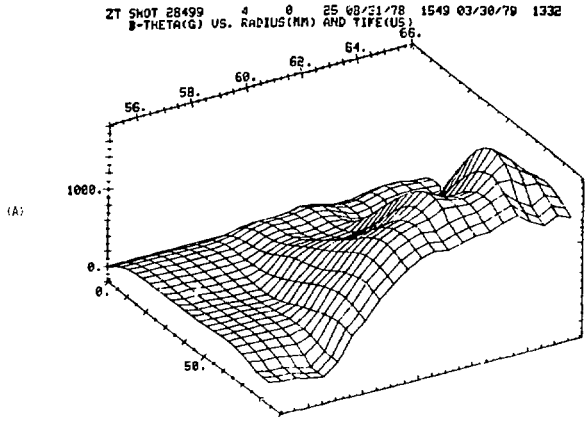

(A)

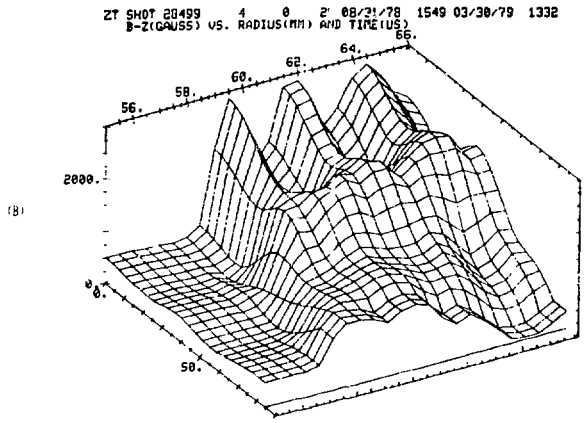

(B)

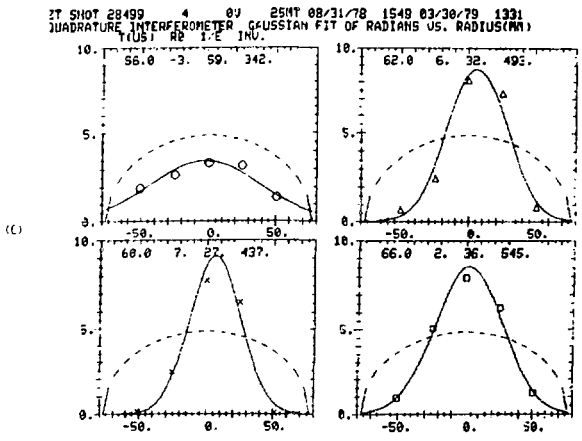

(C)

Fig. 3. Similar to Fig. 2, but shot 28499.

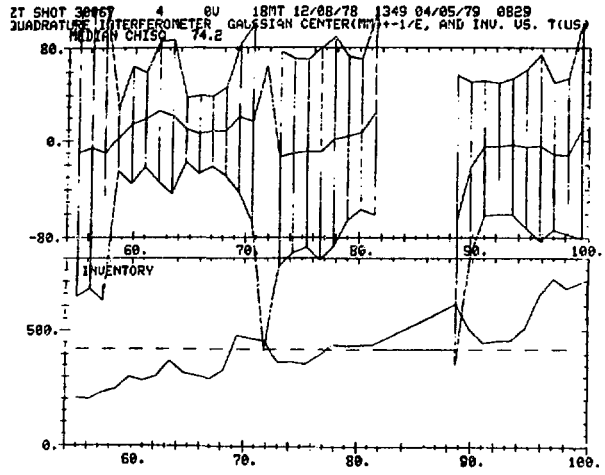

Fig. 4. Density "streak," and line density versus time, for shot 30067.

The main discharge begins at t = 57 μs. For the next 6 μs, there is a very pronounced outward toroidal shift which, as mentioned earlier, is caused by the failure of j_ϕ to get off the ceramic wall initially. At t = 64 μs there occurs another pinching of the plasma (this time with B_θ penetration), and the toroidal shift is reduced. By t = 70 μs, the plasma expands out to both walls, and thereafter the plasma column is not well defined. Therefore the column confinement is poor in this sort of pitch-programming discharge, barely extending beyond the set-up phase.

It would be of interest to examine the fluctuations δn in the electron density as a function of position in the plasma column. However, the phase shift data is integrated along each of five chords. For coherence lengths shorter than a chord, therefore, the fractional phase fluctuations $\delta\phi/\phi$ represent a lower bound on $\delta n/n$ at the most turbulent point along the chord. With this proviso, the fluctuations $\delta\phi/\phi$ for each of the five chords are seen by superposing data from three shots, as in Fig. 5. The fluctuations (i.e., shot-to-shot irreproduciblities) $\delta\phi/\phi$ approach the order of unity after t = 70 μs. On this shot-to-shot basis the phase shifts are moderately "quiet" only for the first 13 μs of the main discharge.

The pitch-programming discharges exemplified by shot 28499 (see Fig. 1c) have a faster-rising B_θ, so that the plasma is held off the wall better at early times. Figure 6 shows the interferometer "streak" and line density histories for shot 28499. Between t = 60 μs and t = 80 μs, the column drifts toward the inner (in major radius) wall. This drift culminates in a stacking-up of plasma against the inner wall at about t = 88 μs. Afterwards, the column forms again, but with a much wider cross section.

The shot-to-shot behavior of seven such shots is shown in the interferometer "streak" superposition of Fig. 7. For simplicity, the centroid has been omitted, so that only the 1/e loci are shown. Apparently there is only 10 μs before large-scale fluctuations (of the plasma boundaries) set in. Although the dominant excursion is inward (in major radius), there is considerable scatter between the behavior of the several shots in Fig. 7. Each of the five interferometer chordal phase shifts are overlaid, for the same seven shots, in Fig. 8. Significant ($\delta\phi/\phi \gtrsim 0.5$) fluctuations occur after t = 70 μs. In the channels on the wings (at $R - R_o = \pm 5.1$ cm), $\delta\phi/\phi \simeq 1$.

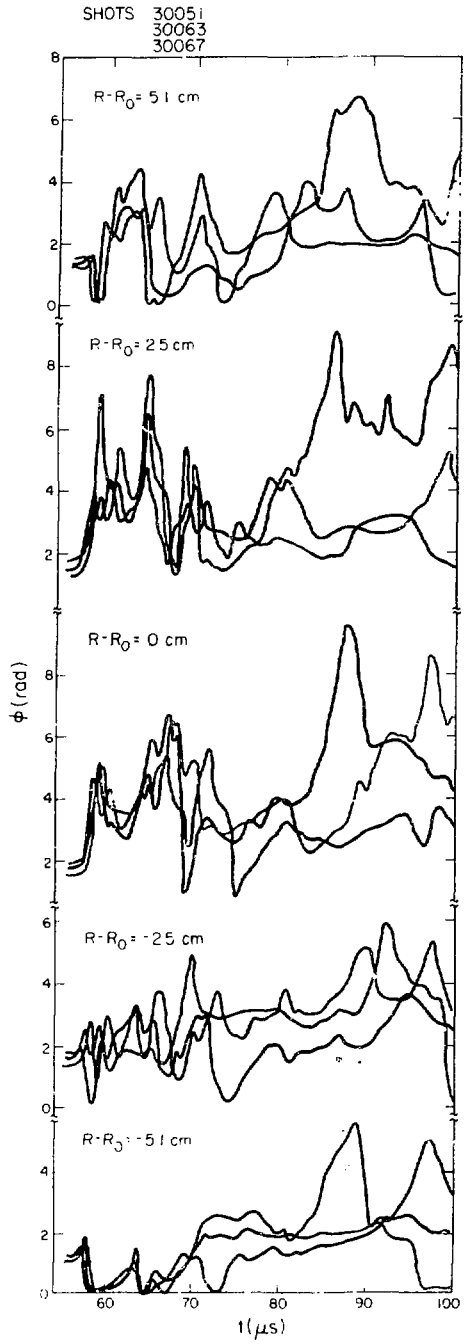

Fig. 5. Interferometer signals recorded simultaneously at five chords for three similar shots with high inductance in the B_θ primary. The three data records at each chord are irreproducible for t > 70 μs.

D. Observed Magnetic Field Structure in Pitch-Programming Discharges

A universal feature of discharges on the upgraded ZT-S device is a toroidal field that peaks strongly on axis and decreases more or less monotonically at larger minor radii. This is shown in Fig. 9a for the first

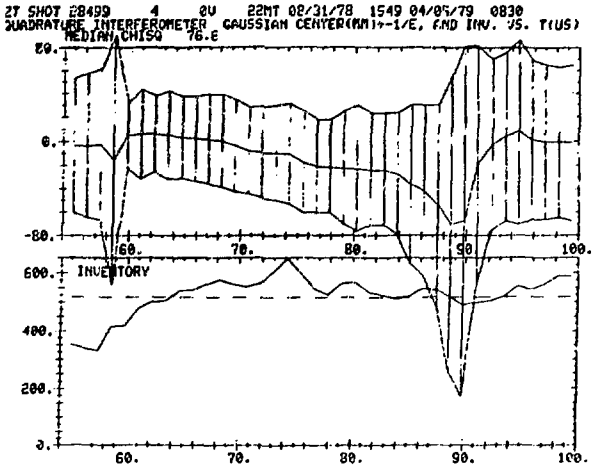

Fig. 6. Density "streak" and line density versus time, for shot 28499.

example, shot 30067. Even during the pre-ionization phase (between t = 0 μs and t = 56 μs) there is considerable peaking of the toroidal bias field. The initial equilibrium is θ-pinch-like, so that for the first several microseconds after t = 56 μs there is a diamagnetic dip of B_ϕ on axis. However, after t = 63 μs, the toroidal field peaks on axis and remains that way for the next 60 μs. (At t = 126 μs the analog-to-digital converters fill up, terminating the probe signal records.) It should be recalled that the interferometer data for shot 30067 (see Fig. 4) show no such enduring structure in the density profile. That is, the well-ordered B_ϕ profile of Fig. 9a apparently coexists with the chaotic density behavior shown in Fig. 4. (This should serve as a caveat against concluding that a shot is "stable" solely on the basis of the lifetime of the toroidal field profile.)

The evolution of the poloidal field profile for shot 30067 is shown in Fig. 9b. The delayed inrush of B_θ is apparent, after which a rather narrow (~ 3 cm radius) current channel sets up and lasts for the duration of the record. It is also apparent that the radial fall-off of B_θ (outside the main current channel) is weaker than 1/r, so that a true "vacuum" region does not exist.

Both field components' profiles are shown in Fig. 10 (a and b) at the single time, t = 80 μs. The toroidal field shows the typical peaked distribution. The field reversal does not penetrate inward of r = 5.8 cm.

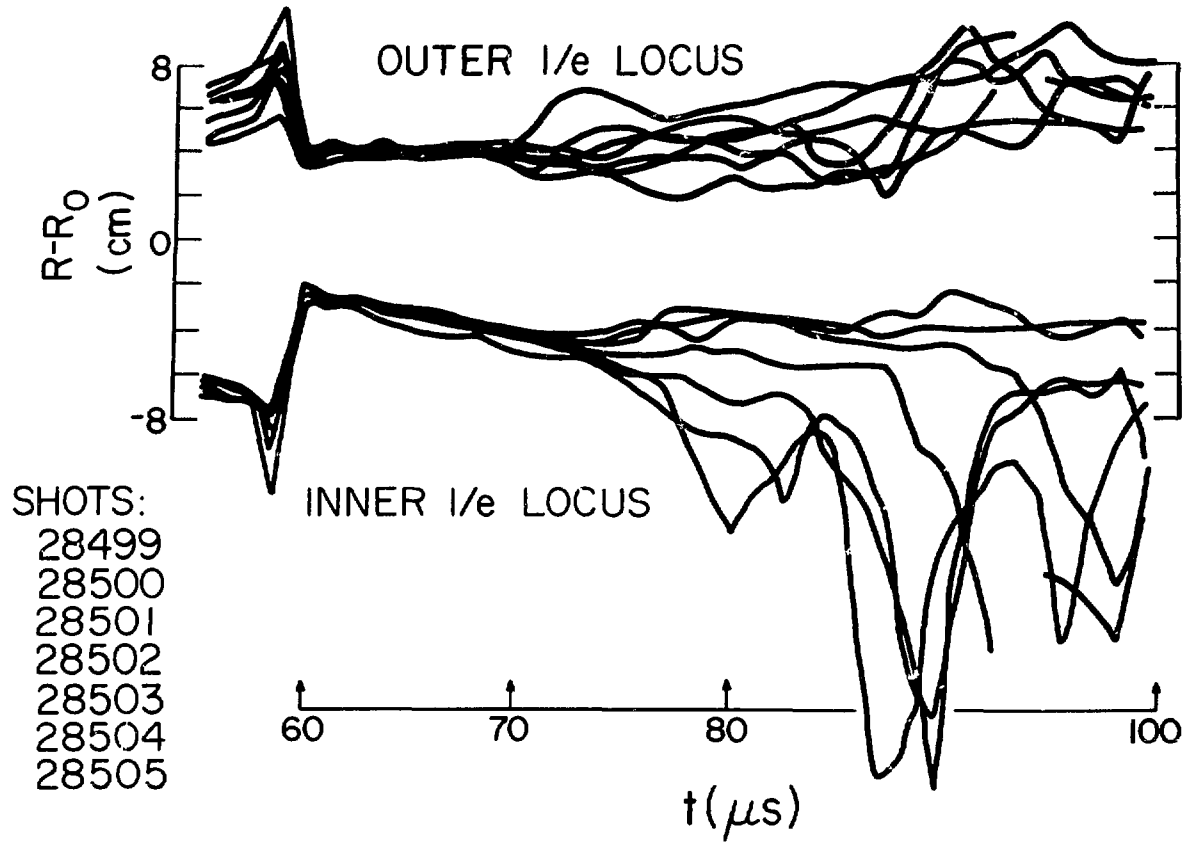

Fig. 7. Overlay of density "streaks" (without centroid) for seven consecutive shots with low inductance in the B_θ primary.

The toroidal current channel, mentioned above, is narrow (a ≃ 3 cm), as can be seen in Fig. 10b.

The shot-to-shot fluctuations in the magnetic fields, for three identical discharges including shot 30067, are shown in Fig. 11 (a and b). As with the interferometer phase shift fluctuations, t = 70 μs apparently is the onset of irreproducible fluctuations. However, unlike the phase fluctuations, those associated with the fields are superposed on a reproducible structure. In other words, $\delta B/B \lesssim 0.3$, whereas $\delta\phi/\phi \simeq 1$.

The second example, shot 28499, has a faster-rising toroidal current; the field histories are shown in Fig. 12 (a and b). One sees that B_ϕ peaks on axis from the start of the main bank (near t = 56 μs), with no transient

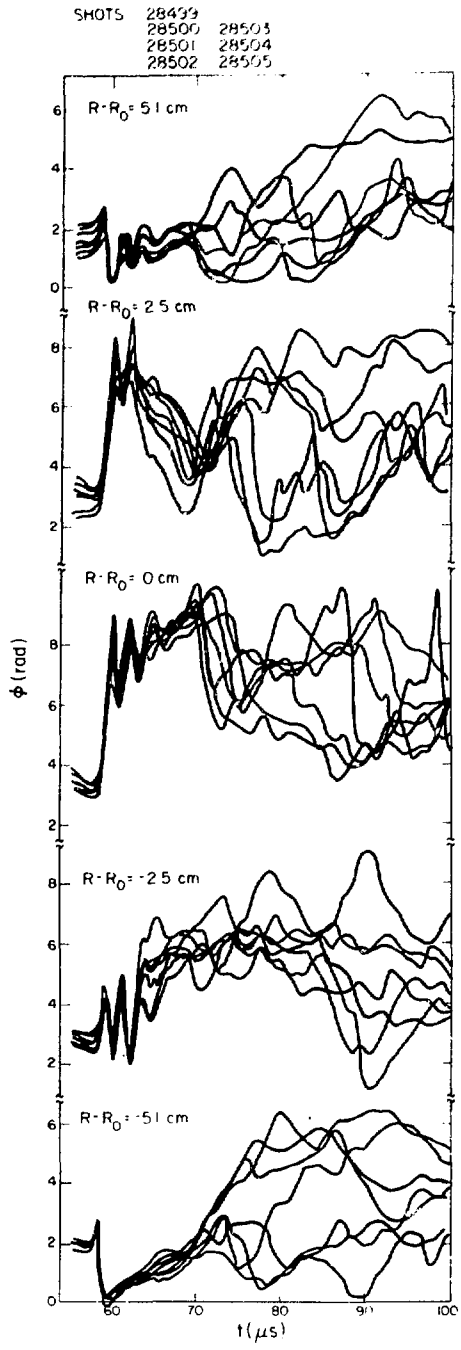

Fig. 8. Similar to Fig. 5, but for the seven shots of Fig. 7. The data records at each chord are irreproducible after t = 70 μs.

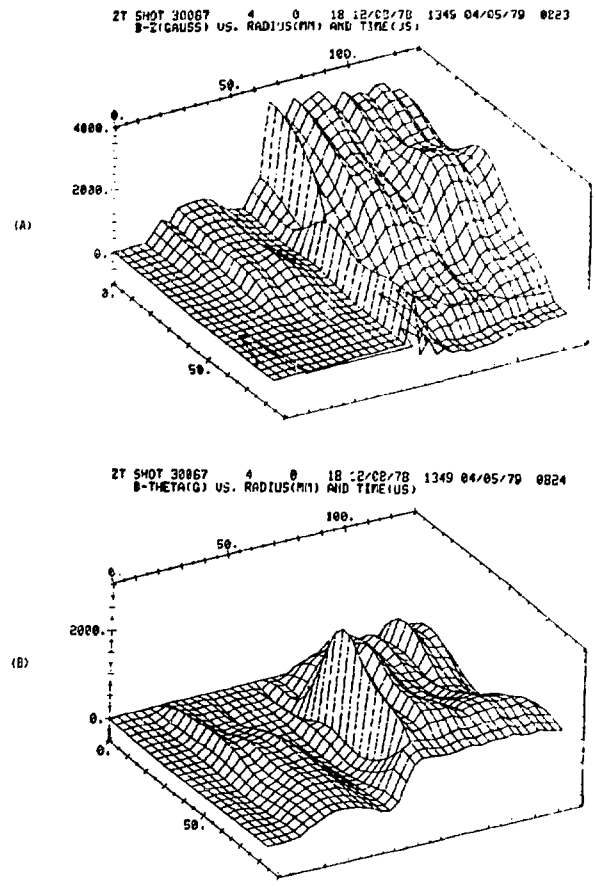

Fig. 9. (a) Toroidal field (gauss, vertical scale) versus minor radius (mm, lower scale) and time (μs, upper scale) for shot 30067. The preionization phase is before t = 56 μs.
(b) Similar, but poloidal field.

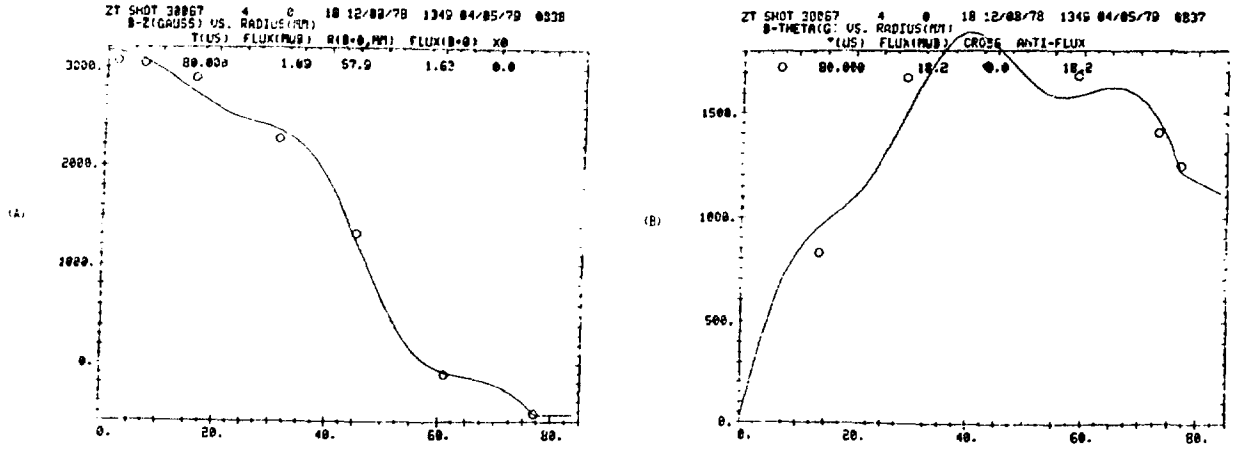

Fig. 10. (a) Toroidal field (gauss) versus minor radius (mm) at t = 80 μs, or t_o + 24 μs.
(b) Similar, but poloidal field.

θ-pinch-like equilibrium. Likewise, there is substantial initial penetration of B_θ. (This is a consequence of $\dot{B}_\theta$ being comparable to $\dot{B}_\phi$ during the first rise.)

The field profiles for shot 28499 at t = 80 μs are shown in Fig. 13 (a and b). The toroidal field at the wall is not reversed, but the peaked B_ϕ profile otherwise is similar to shot 30067. The toroidal current channel is apparently wider (a ≈ 4 cm) than with shot 30067.

The field fluctuations for shot 28499 and six other identical discharges are shown in the overlay plots of Fig. 14 (a and b). The fractional variations $\delta B/B$ are significantly smaller than $\delta\phi/\phi$ for the same discharges (see Fig. 8).

E. Conclusions on Pitch Programming

The experiments described above do not provide a definitive test of the pitch-programming concept. The actual waveforms (in B_ϕ and B_θ) employed do not have the speed and shape that are considered necessary to explore the pitch-programming mode of operation.

In order to improve the resemblance between experiment and model, it would probably be necessary to change from the toroidal field windings' present configuration (five in series; inductance per quadrant ≈ 1300 nH) to a faster arrangement (all turns in parallel; L ≈ 250 nH). The time-to-crowbar

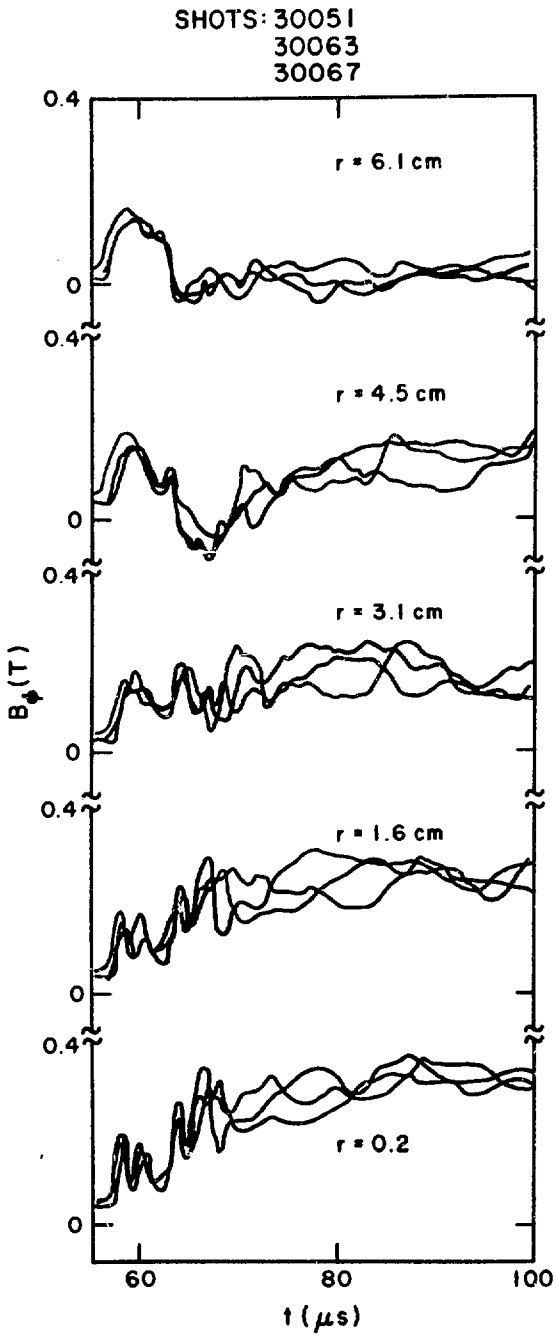

Fig. 11. (a) Overlay of toroidal field traces (at five positions in minor radius), for three similar shots.

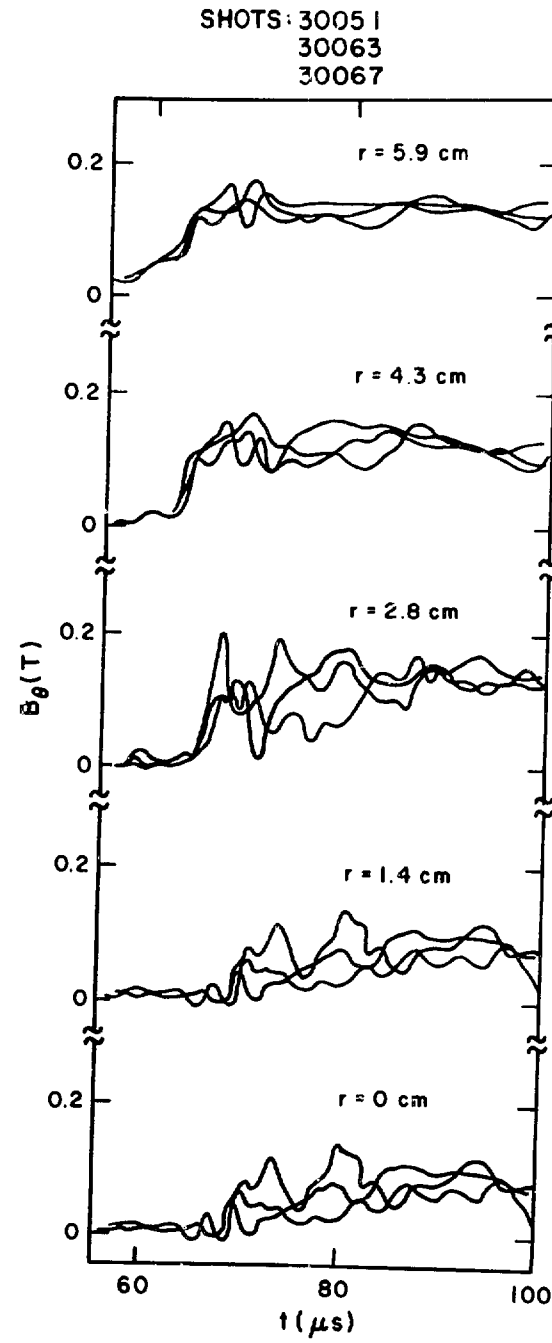

Fig. 11. (b) Similar, but poloidal field.

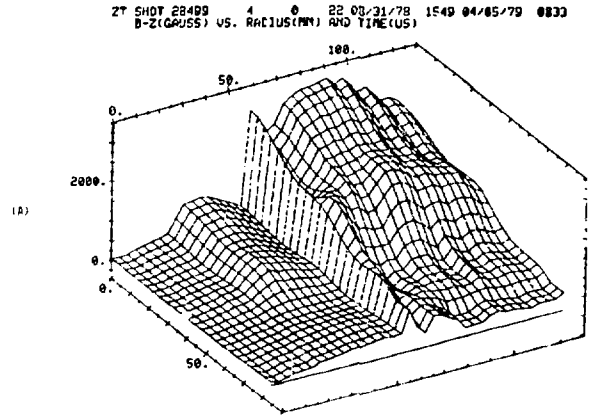

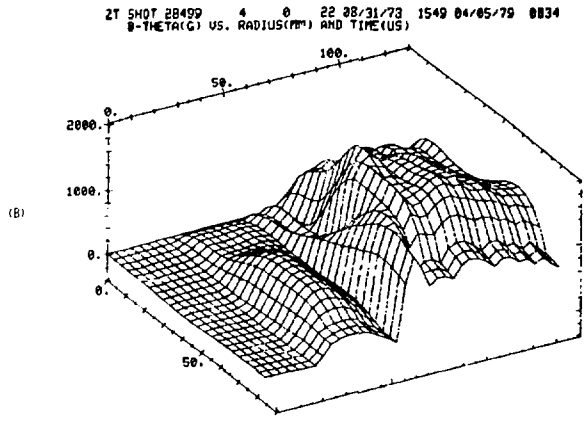

Fig. 12. (a) Toroidal field (gauss, vertical scale) versus minor radius (mm, lower scale) and time (μs, upper scale) for shot 28499. (b) Similar, but poloidal field.

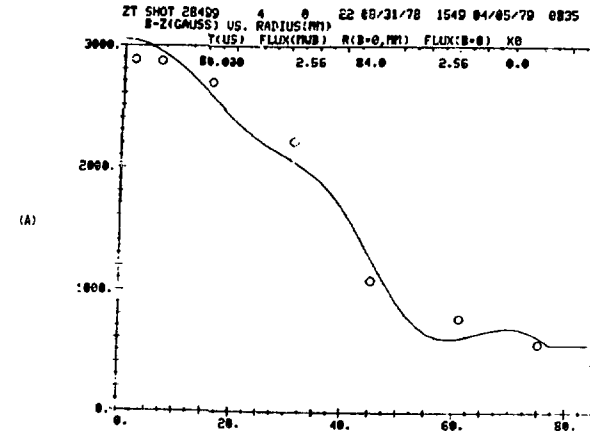

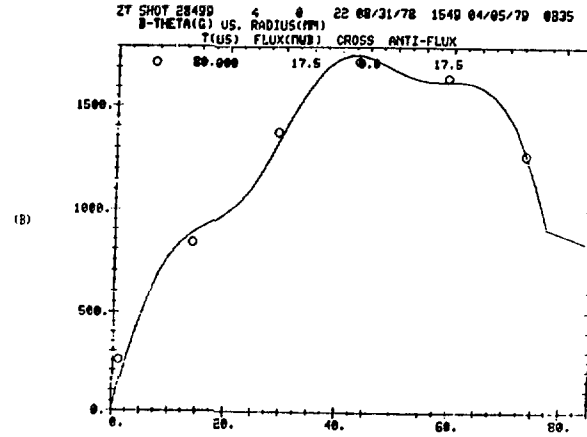

Fig. 13. (a) Toroidal field (gauss) versus minor radius (mm) at t = 80 μs. (b) Similar, but poloidal field.

would then be approximately 4 μs, compared to the present 9 μs. It is an open question, however, whether this modification would be sufficient since the plasma bouncing can still be expected to distort the toroidal field waveform (relative to its vacuum shape).

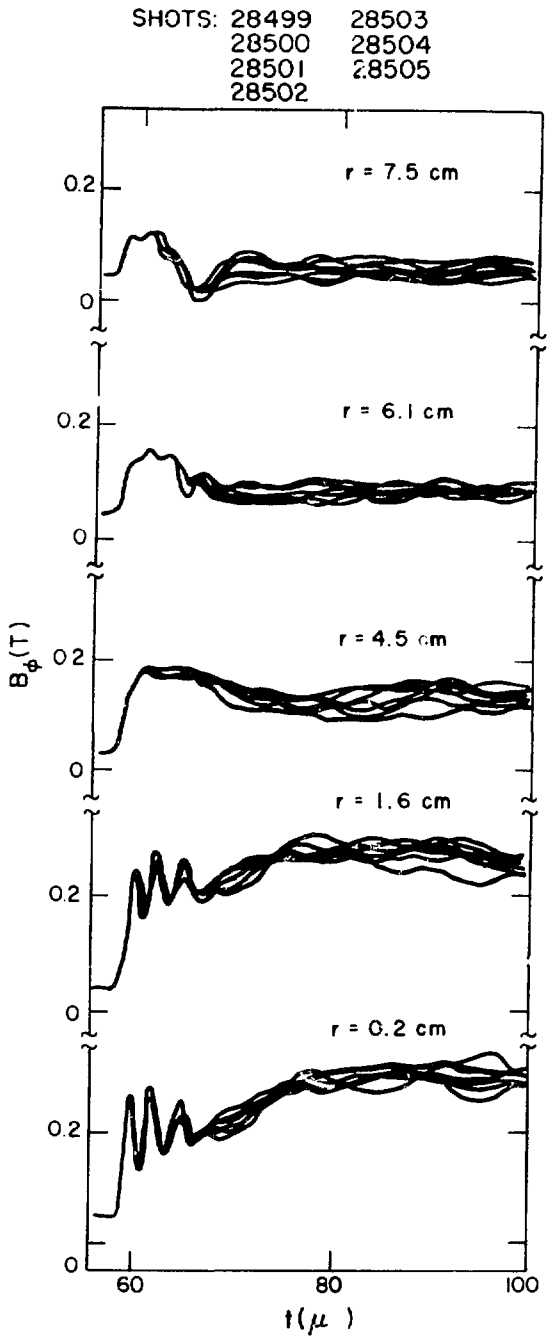

Fig. 14. (a) Overlay of toroidal field traces (at five locations in minor radius), for seven similar shots.

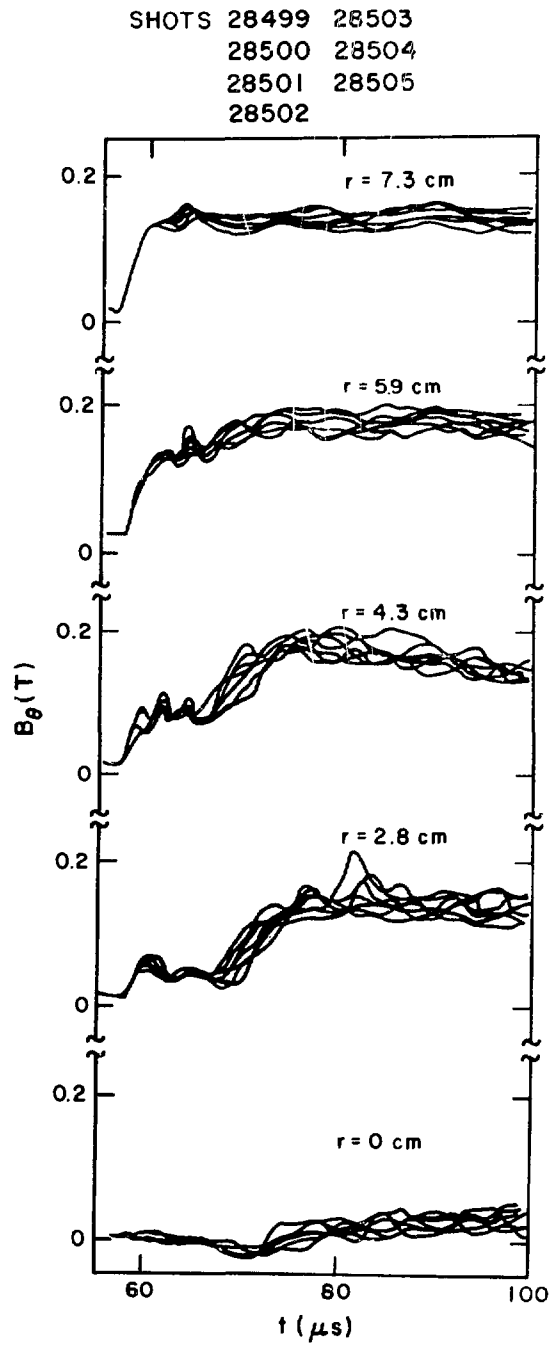

Fig. 14. (b) Similar, but poloidal field.

III. THE OBSERVED LONG-LASTING TOROIDAL FIELD PROFILES

A. Introduction

As discussed in the previous section, the qualitative features of the toroidal field profile are insensitive to the detailed setting-up and stability of the discharge. B_ϕ peaks on axis and tapers more or less monotonically to zero at the wall, and this profile generally flattens by less than 30% over the next 60 μs for which data is recorded.

Logically, there could be at least three causes for this behavior of the toroidal field profile:

1) The peaked B_ϕ profile is built into the plasma during the set-up phase and then maintained for a diffusion time.
2) The plasma assumes a gross helical kink configuration, with the resulting solenoid field peaking on axis.
3) The plasma is extremely paramagnetic.

[It should be noted that (2) and (3) are mechanisms for the toroidal current circuit to drive the toroidal field.]

B. Experimental Test of the Diffusion Mechanism

If diffusion controls the lifetime of the peaked B_ϕ profile, then depressing the electron temperature (via the addition of known quantities of nitrogen) ought to shorten that lifetime. Such an experiment was performed on a discharge with fast toroidal current rise (similar to the example shot 28499, described in Fig. 1c and elsewhere in Section II). Three identical discharges will be discussed below:

1) Shot 29070 (25 mtorr H_2).
2) Shot 29074 (25 mtorr H_2 + 1.25 mtorr N_2).
3) Shot 29075 (25 mtorr H_2 + 5.0 mtorr N_2).

The toroidal field structures of all three shots are grossly similar, as can be seen in Fig. 15 (a, b, and c). The radial profiles at three times are more quantitatively compared in Fig. 16 (a, b, and c). The peak values of B_ϕ on axis are reduced by less than 15% in going from pure H_2 to a 20% nitrogen impurity addition to the gas fill.

The density "streak" and inventory histories for this series of shots are shown in Fig. 17 (a, b, and c). As an aside, it should be noted that the pre-ionization discharge (25 μs < t < 58 μs) becomes substantially stabilized by the addition of nitrogen impurity. This can be accomplished alternatively by simply using a higher filling density of pure H_2, so the stabilization

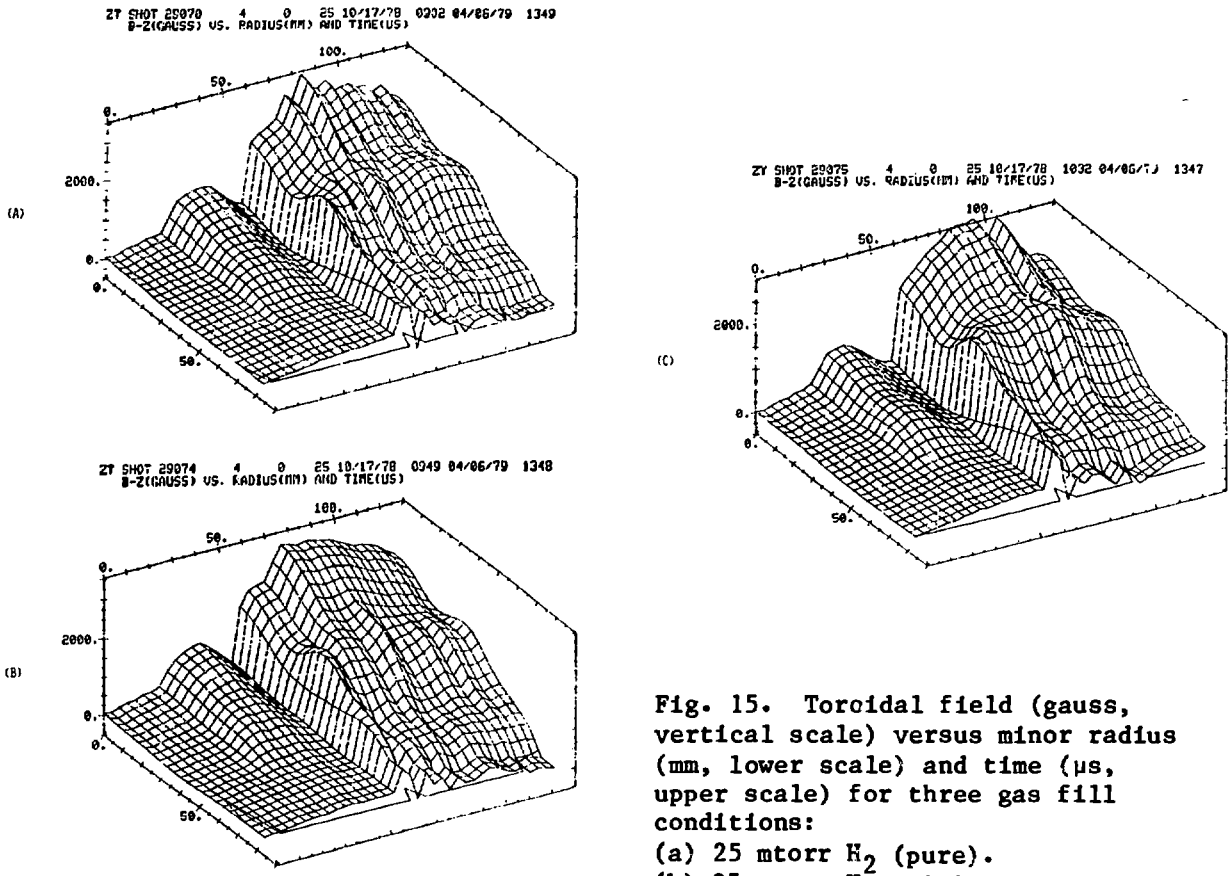

Fig. 15. Toroidal field (gauss, vertical scale) versus minor radius (mm, lower scale) and time (μs, upper scale) for three gas fill conditions:
(a) 25 mtorr H_2 (pure).
(b) 25 mtorr H_2 + 1.25 mtorr N_2.
(c) 25 mtorr H_2 +5.0 mtorr N_2.

might be due to increased mass loading of the column. For the purpose of the diffusion experiment, though, the information of most interest is the peak inventory (line density) achieved during the main discharge. The dashed line corresponds to 100% ionization of 25 mtorr H_2. In shot 29070, the line density peaks at 8% above the hydrogen level. In shot 29075, on the other hand, the line density peaks at 29% above the hydrogen level. This is consistent with the nitrogen additive (20% of hydrogen) being singly ionized (within the estimated 5% uncertainty with which the interferometer system measures the inventory). This experimental observation will be used below to test the validity of a computer model.

An upper bound for the electron temperature in shot 29075 can be estimated using a zero-dimensional computer code[6] implementing the collisional-radiative[7] model. (That the estimate is probably an upper bound

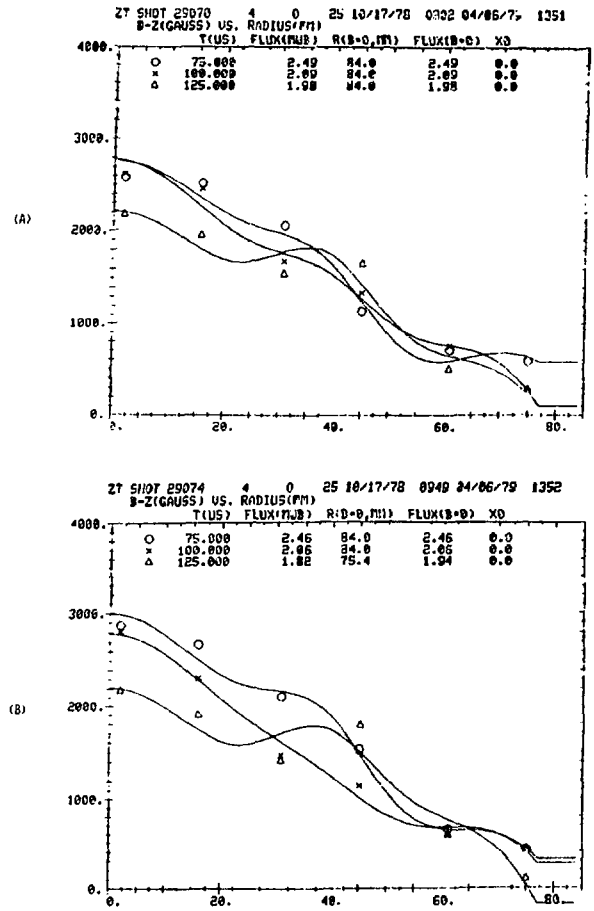

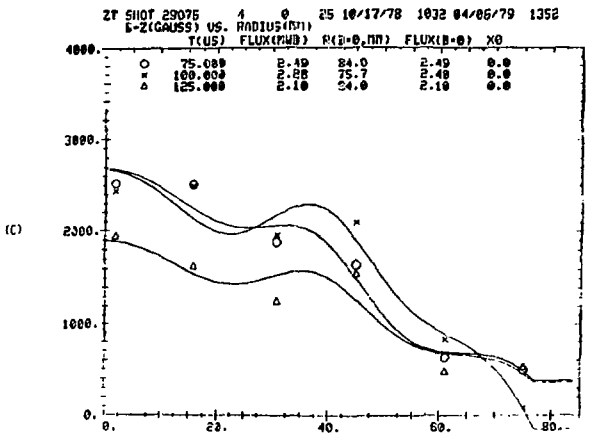

Fig. 16. Toroidal field (gauss) versus minor radius (mm) at three times for three gas fill conditions:
(a) 25 mtorr H_2 (pure).
(b) 25 mtorr H_2 + 1.25 mtorr N_2.
(c) 25 mtorr H_2 + 5.0 mtorr N_2.

is due to the fact that the zero-dimensional calculation ignores conductive and convective heat losses.) Care will be taken to verify that the estimate is otherwise insensitive to the inadequacies of the model. The code balances ohmic heating against radiation losses.

The computer code uses a 20% oxygen impurity, but for the first three ionization states, nitrogen is almost exactly as effective in clamping the temperature. Table I shows the similarity in ionization potentials[8] of the two atoms.

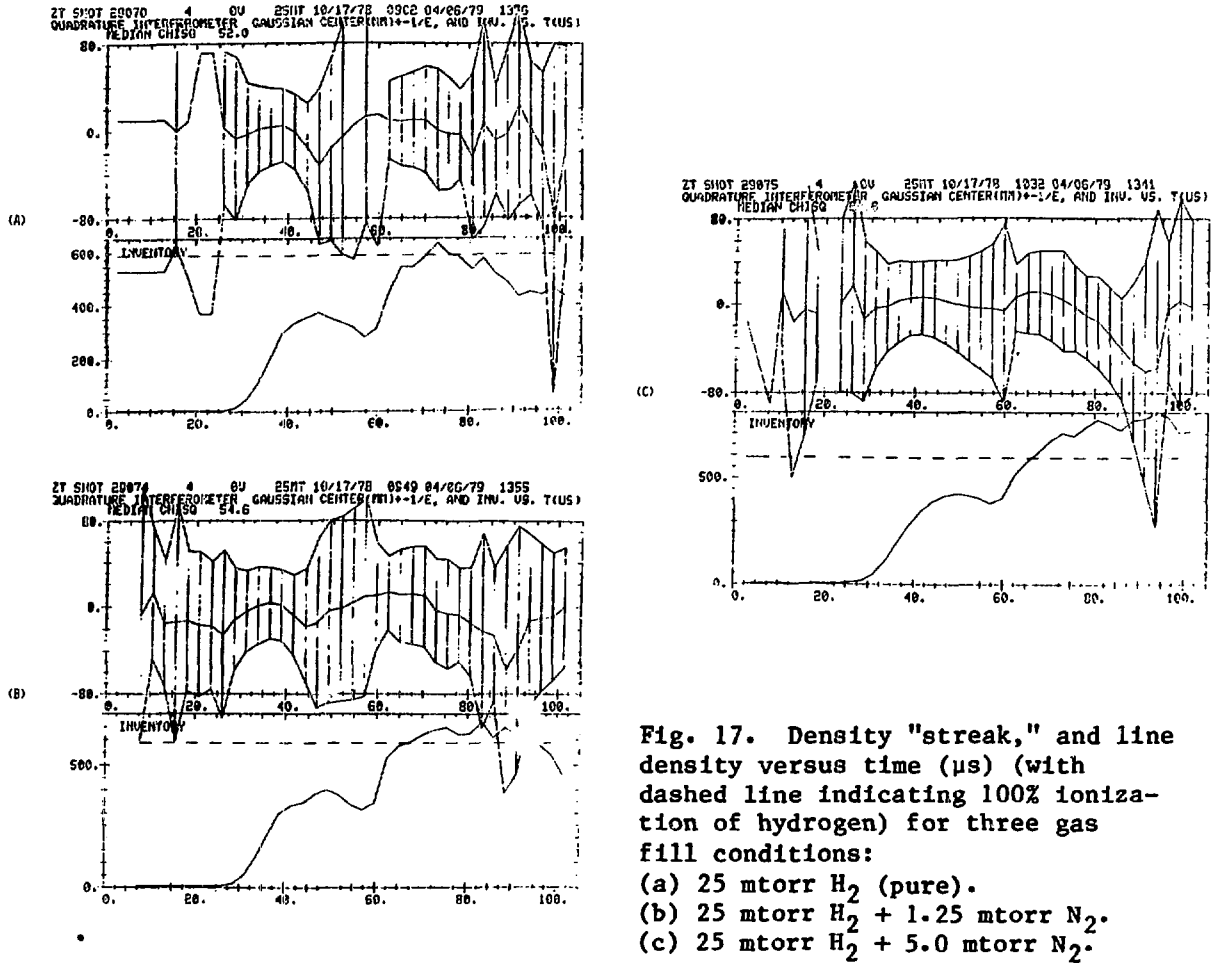

Fig. 17. Density "streak," and line density versus time (μs) (with dashed line indicating 100% ionization of hydrogen) for three gas fill conditions:
(a) 25 mtorr H_2 (pure).
(b) 25 mtorr H_2 + 1.25 mtorr N_2.
(c) 25 mtorr H_2 + 5.0 mtorr N_2.

TABLE I
IONIZATION POTENTIALS OF DIFFERENT IONIZATION STATES (eV)

	I	II	III
nitrogen	14.5	29.6	47.4
oxygen	13.6	35.1	54.9

(There exists a corresponding similarity for the effective oscillator strengths of oxygen and nitrogen in the first three ionization states.)

The total current density can be inferred from the magnetic field profiles of Fig. 18 (a and b) for shot 29075. Choosing t = 75 μs, it is apparent that $0.75 \frac{ka}{cm^2} < j_{total} < 1.75 \frac{ka}{cm^2}$. The electron density can be seen from Fig. 19. The phase shift profile for t = 75 μs Abel inverts into a

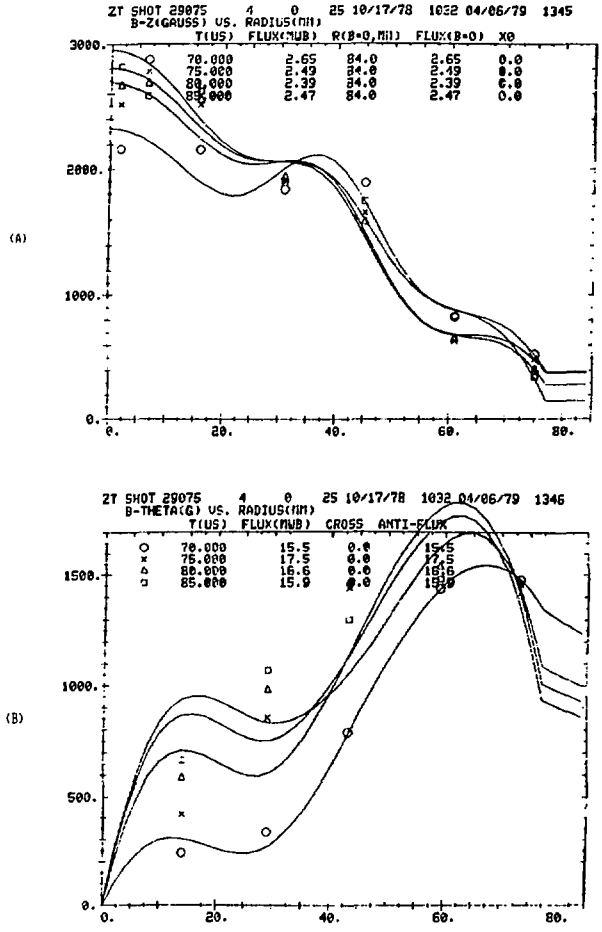

Fig. 18. (a) Toroidal field (gauss) versus minor radius (mm) at four times during nitrogen-poisoned discharge (shot 29075). (b) Similar, but poloidal field.

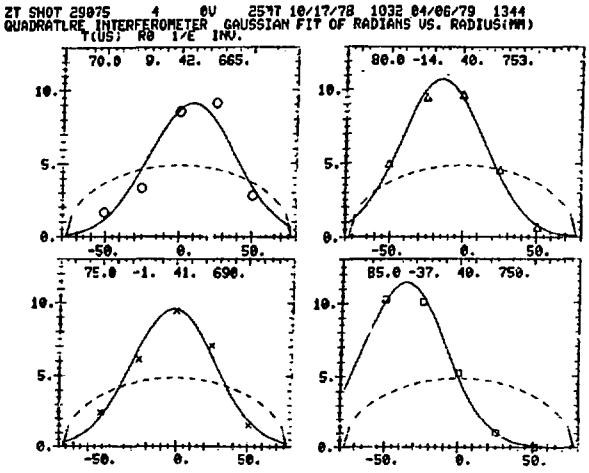

Fig. 19. Interferometer signals along five chords at four times during nitrogen-poisoned discharge (shot 29075). Dashed curve would be expected locus of data if 25 mtorr H_2 were fully ionized and uniformly distributed.

gaussian profile of n_e versus minor radius, with 1/e width 4.1 cm and peak density 5×10^{15} cm^{-3}.

The computer calculations show that within 5 μs after t_o, the 20% impurity effectively clamps the electron (and ion) temperature. Furthermore, this thermostated level is insensitive to the initial choice of electron temperature between 1 eV < T_e < 10 eV. The asymptotic electron temperature and percent of impurity that is singly ionized are shown in Table II. The range of electron density and current density covers all points in the experimental profiles (see above).

Thus, applying the zero-dimensional model to the local electron and current densities found in the experimental profile, it appears that 2.5 eV < T_e < 4.5 eV. This range is narrow enough to suggest that profile effects are not very important here in calculating the radiation-limited temperature. Furthermore, the calculated percent of impurity that is singly ionized is consistent with the experimental observation (see above) from Fig. 17c, thereby enhancing the credibility of the calculation.

The upshot of the computer model is that $T_e \simeq 3.5$ eV, which gives $\eta \simeq 1.6 \times 10^{-4}$ ohm-meters. The classical magnetic diffusion constant is then

$$D = \frac{\eta}{\mu_o} \simeq 1.3 \times 10^2 \ m^2/s$$

TABLE II

ASYMPTOTIC T_e/PERCENT SINGLY IONIZED NITROGEN

(calculated)

j_{tot} $(\frac{ka}{cm^2})$

		0.5	1.0	2.0
n_e (cm^{-3})	1×10^{15}	3.4 eV/99%	4.5 eV/91%	
	3×10^{15}	3.0 eV/99%	3.0 eV/99%	3.7 eV/93%
	5×10^{15}		2.5 eV/100%	3.1 eV/98%

From the data of Fig. 18 (a), the toroidal field profile can be approximated by a pedestal plus Bessel function:

$$B_\phi|_{75\ \mu s} \simeq \left[0.04 + B_\phi(0) J_o\left(2.4\ \frac{r}{0.077\ m}\right)\right] \text{ (Tesla)}$$

The radially varying component (second term) should decay in time with a characteristic period

$$\tau \simeq \frac{1}{2.4^2}\ \frac{0.077^2\ (m^2)}{D}$$

$$= 7.9 \times 10^{-6}\ s$$

That is, the upper bound on the classical toroidal magnetic field diffusion time is 8 μs. (Including the effects of non-radiative losses on T_e and of non-classical processes on η would produce a calculated diffusion time less than 8 μs.)

The experimental profiles (including shot 29075), however, have peaked toroidal profiles that require more than 60 μs to decay. It is unlikely, then, that the plasma's diffusion properties can account for the long lasting toroidal field profiles, at least on those shots in which impurities were added to clamp the temperature. There must be another mechanism.

C. Conditions for the Toroidal Current Circuit to Drive the Toroidal Field Profile

As mentioned earlier, either a gross plasma helical deformation, or microscopic paramagnetism ($\sigma_\parallel/\sigma_\perp \gg 1$) could provide a mechanism for the toroidal current circuit to maintain the peaked toroidal field profile. The toroidal field generated in such a way could be steady state, not limited by a diffusion time.

In regard to the gross helical kink mechanism, it is illuminating to consider the pitch required of a "toroidal" current filament to support the observed on-axis toroidal field. A typical value of B_ϕ on axis (in the observed peaked profiles) is 0.3 Tesla. The toroidal current in such a

discharge is typically 50 kA. This implies that the average pitch of a current filament (in order for the B_ϕ peak on axis to be solely generated by a helical deformation of I_ϕ) would be 4.8 revolutions per meter (or 12 revolutions during one transit around the torus). While such deformations are frequently observed on a toroidal pinch (by Fourier probes and streak photography), they are transient and unlikely to remain stationary for the 50 μs (and more) required to explain the long lasting toroidal field profiles reported here.

Another mechanism by which I_ϕ can support the peaked B_ϕ profile is microscopic paramagnetism of the plasma. Field profiles in the paramagnetic model have been numerically calculated by Haberstich.[9] Comparing shot 29070 (see above) to those calculations, it appears that $\sigma_\parallel/\sigma_\perp \gtrsim 5$ would be required to account for the field structure properties.

The above argument is not meant to imply that gross kink deformations cannot play a role in toroidal flux enhancement during ZT-S discharges. Verhage et al.[10] have observed a buildup of toroidal flux inside of the reversal point by precisely such a mechanism. Although the range of toroidal currents has been too limited to achieve sustained self-reversal of the toroidal field, ZT-S has exhibited a similar mechanism for generating toroidal flux. For example, a series of stabilized pinch discharges (initial B_ϕ = 300 gauss) have been observed to undergo strong toroidal flux enhancement associated with a violent instability. The toroidal and poloidal field histories during the first 12 μs of such a discharge are shown in Fig. 20 (a and b). The toroidal current rises to 58 kA in 4.5 μs and is then crowbarred. The data for B_θ at the outermost (r = 77 mm) end of the radial profiles is determined from an internal probe, and it agrees well (until t = 64.5 μs) with the toroidal current. Between t = 60 μs and t = 64.5 μs, the plasma column sits quietly in a highly compressed state. (The streak picture and interferometer data confirm this.) At t = 64.5 μs a large-scale redistribution of the fields takes place. The Fourier coils on ZT-S were not operational, so direct magnetic evidence for a helical deformation was not available. However, both the streak camera and interferometer data indicate that plasma abruptly hits the wall, and then more-or-less uniformly fills the tube, between t = 64.5 μs and t = 67 μs. Furthermore, there is an additional bit of evidence, from the field profile itself, of gross plasma motion. During the field redistribution period (t = 64.5 μs to t = 67 μs) the poloidal

field, measured by an internal probe near the wall, dips by about 30%. However, the toroidal current (not shown) exhibits no such transient decrease. This sets a lower limit on the transient displacement of the centroid of the toroidal current in the (ϕ = constant) plane containing the probe: $(\Delta r)_{min} \simeq 2.2$ cm.

The toroidal and poloidal fluxes are shown in Fig. 21 (a and b). Their behavior up to t = 64 μs can be explained by plasma compression and a modest amount of paramagnetism (in the toroidal flux). During the unstable stage (between t = 64.5 μs and t = 67 μs) the toroidal flux more than doubles, and the poloidal flux is reduced. (It should be mentioned that the toroidal flux is not crowbarred until t ≃ 71 μs, so that flux is available from the circuit during the instability.) At the peak of the instability, the flux measurements are inaccurate, because they rely on axisymmetry. However, by t = 70 μs, by which time the plasma is centered again in the tube, the computed fluxes are accurate to within 10%. Between t = 64 μs and t = 70 μs, the net change in toroidal flux is 1.4 mWb. Using the lower bound on helical displacement ($\Delta r \gtrsim 2.2$ cm) deduced above (at the height of the unstable phase), this flux jump can be used to estimate an upper bound on the helical wave number:[11] $k \lesssim 6.3\ m^{-1}$. Thus the net toroidal flux jump is consistent with a helical wavelength of the order of, or greater than, one meter. The major perimeter of the torus is 2.5 meters; thus $q \gtrsim 0.4$ for the inferred helix. On the other hand, the magnetic field equilibrium at 64 μs, immediately prior to the unstable motion, has $q \lesssim 0.12$, as can be seen in Fig. 22. Thus, it does not appear likely that the inferred helical deformation's pitch matches the equilibrium pitch, assuming that the toroidal flux jump is generated by the helical instability.

The rapid enhancement of toroidal flux in shot 29183 causes an equally rapid approach to the Taylor curve for $\beta = 0$. The "F-θ" coordinates are shown in Fig. 23 at 2 μs intervals. Before the instability, the plasma sits out on the right, at $\theta \simeq 2.5$. Between t = 64 μs and t = 68 μs, the plasma joins the Taylor curve by reducing the pinch ratio. Thereafter the F-θ locus meanders slowly down the curve.

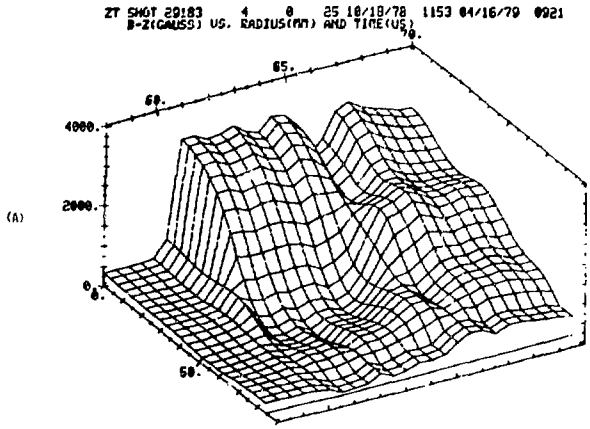

Fig. 20. (a) Toroidal field (gauss, vertical scale) versus minor radius (mm, lower scale) and time (μs, upper scale) during the dynamic phase of a stabilized pinch discharge (shot 29183).
(b) Similar, but poloidal field.

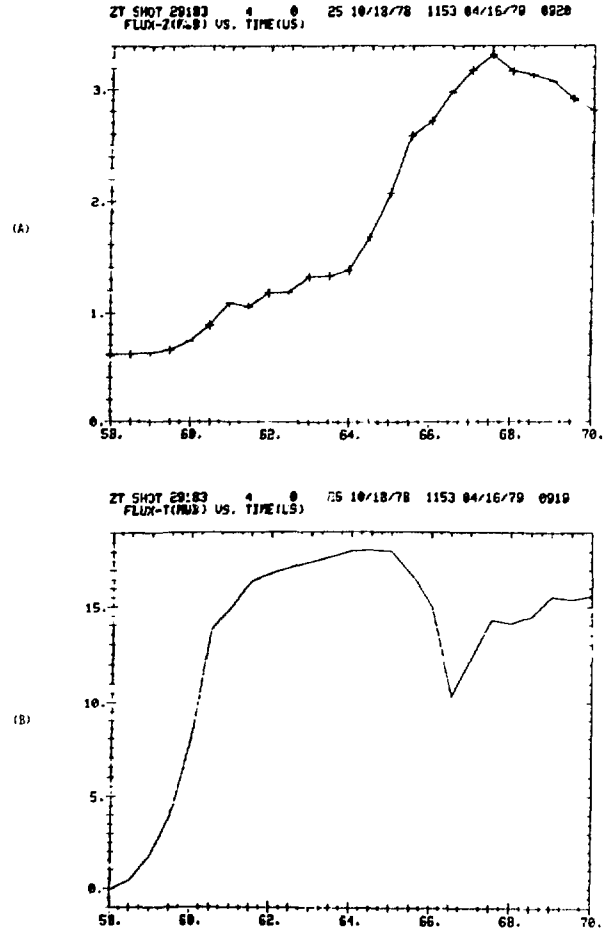

Fig. 21. (a) Toroidal flux (milliweber) versus time (μs) during the dynamic phase of a stabilized pinch discharge (shot 29183).
(b) Similar, but poloidal flux. The transient drop during 56 μs < t < 67 μs is an artifact of temporary displacement of the plasma column.

IV. POSSIBLE SHEAR ALFVEN WAVES DUE TO TOROIDAL EFFECTS

A. Introduction

Shear Alfvén waves propagate locally along magnetic field lines. A perturbation of given frequency and wavevector tends to propagate along those

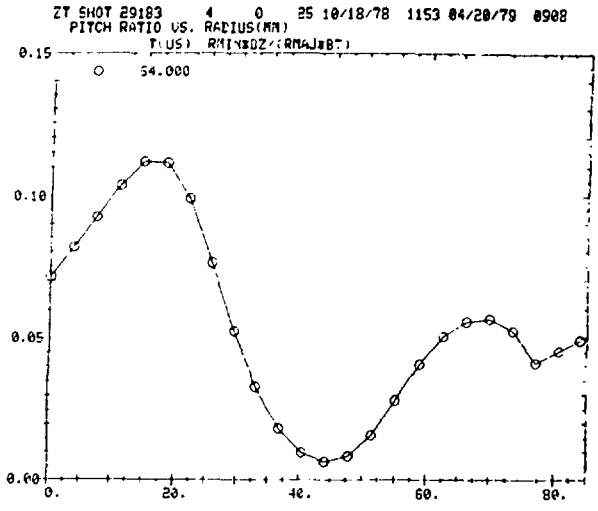

Fig. 22. Safety factor ($q \equiv rB_\phi/RB_\theta$) versus minor radius (mm) immediately prior to instability in a stabilized pinch discharge (shot 29183). The curve is constructed from spline fits to six B_θ data points and six B_ϕ data points.

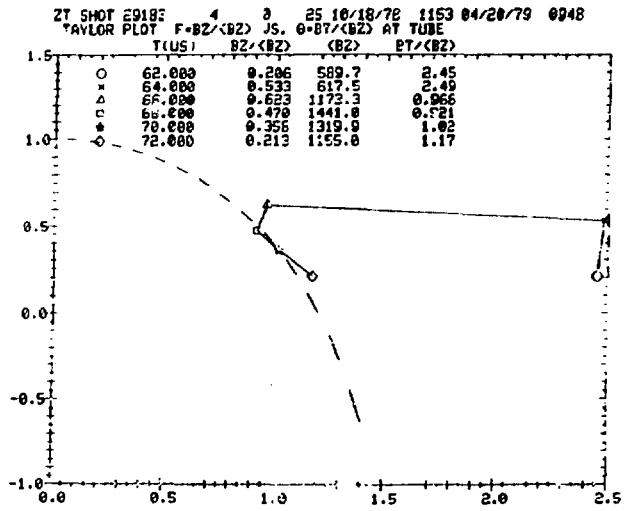

Fig. 23. F-θ diagram for the dynamic phase of a stabilized-pinch discharge (shot 29183). The instability occurring between t = 64 μs and t = 66 μs returns the pinch to the vicinity of a β = 0 Bessel function model (dashed curve).

field lines where the local Alfvén speed matches the phase speed of the wave (parallel to the field).[12]

A cylindrical pinch has (by definition) a cylindrically and axially symmetric equilibrium. All variation is along r, while z and θ are ignorable. If one were to excite such a pinch with a launching structure that also has $m = 0$, $k_z = 0$ symmetry, then no shear Alfvén waves would be expected, since $\vec{k} \cdot \vec{B} = 0$ (due to fact that $B_r = 0$).

In a torus, the equilibrium has a built-in $m = 1$ distortion that increases with tighter aspect ratio. If one follows a field line once around the minor cross section (that is, through $\Delta\theta = 2\pi$), the local pitch will be modulated with periodicity 2π (in the coordinate θ), which is $m = 1$. The associated k_ϕ for that field line depends on the <u>average</u> pitch.

This intrinsic $m = 1$ distortion in toroidal pinches may provide a mechanism for launching Alfvén waves in an axisymmetric toroidal pinch. On the one hand, this may complicate the magneto-acoustic heating schemes

contemplated with m = 0, k = 0 symmetry. On the other hand, Alfvén wave heating in a tight aspect ratio torus may be possible even with nominally "m = 0, k = 0" excitation (which would consist just of oscillating the currents in the transformer primaries). Furthermore, shear waves, which might naturally occur in toroidal axisymmetric plasmas, may help to account for certain experimental observations.

Define:

$$B \equiv \left(B_\theta^2 + B_\phi^2\right)^{1/2} \quad ; \quad \mu \equiv \text{atomic mass}$$

$L \equiv$ distance for a field line to travel $\Delta\theta = 2\pi$ ("pitch length")

$$L = 2\pi r \frac{B}{B_\theta}$$

The Alfvén speed (per unit magnetic field) is given by

$$\frac{V_A}{B}\left(\frac{\text{cm}}{\text{s - gauss}}\right) = \frac{2.18 \times 10^{11}}{\mu^{1/2}\left[n_i\ (\text{cm}^{-3})\right]^{1/2}}$$

The transit time for an Alfvén wave through $\Delta\theta = 2\pi$ (i.e., a distance L along $\vec{B}$) is

$$\tau_A = \frac{L}{V_A} = \frac{L/B}{V_A/B} = \frac{2\pi r/B_\theta}{V_A/B}$$

Numerically,

$$\tau_A\ (\mu s) = \frac{0.91\ \sqrt{\mu}\ r(\text{cm})\ \left[n_i(10^{15}\text{cm}^{-3}\right]^{1/2}}{B_\theta\ (\text{kG})} \qquad (1)$$

The Alfvén time τ_A thus depends explicitly only on the poloidal, and not the toroidal, field. (However, the two are related by pressure balance.) Consider a pinch with current j_ϕ uniformly filling the interior of radius a and falling to zero for $r > a$. For $r < a$, the "interior" Alfvén time (for traveling $\Delta\theta = 2\pi$ along a field line) reduces to

$$\tau_{A,int}(\mu s) \simeq \frac{4.6\ \sqrt{\mu}\ a^2(cm^2)\ [n_i(10^{15}cm^{-3})]^{1/2}}{I_\phi(ka)} \tag{2}$$

For $r > a$, the "exterior" Alfvén time is

$$\tau_{A,ext}(\mu s) \simeq \frac{4.6\ \frac{r}{a}\ \sqrt{\mu}\ a^2(cm^2)\ [n_i(10^{15}cm^{-3})]^{1/2}}{I_\phi(ka)} \tag{3}$$

B. Possible Implications for Magnetoacoustic Heating

The period τ_B of an $m = 0$, $k_\phi = 0$ radial hydromagnetic oscillation for such a pinch can be estimated as

$$\tau_b(\mu s) \simeq \frac{2\ \sqrt{\mu}\ a^2(cm^2)\ [\bar{n}_i(10^{-15}cm^{-3})]^{1/2}}{I_\phi(kA)} \tag{4}$$

where

$$\bar{n}_i \equiv \int_o^a n_i(r)\ 2\pi r\ dr/(\pi a^2)$$

assuming that most of the line density is within $r = a$, and that only a relatively tenuous plasma lies outside the current channel. Equation (3) is roughly (to within ± 20%) correct for cases of practical interest.

Both Eqs. (2) and (4) scale the same way with pinch radius and current. In order for the radial m = 0, k = 0 motion to launch an Alfvén wave interior to r = a, the periods given in Eqs. (2) and (4) must be equal. This occurs when

$$n_i \approx \frac{\bar{n}_i}{5.3}$$

Inside r = a, such a condition on the density is not likely to be satisfied. Thus it is extremely improbable that the radial magnetoacoustic wave will couple to an Alfvén wave (of the sort considered here) within the current channel.

Outside the current channel, however, the density can become sufficiently low (and the Alfvén speed correspondingly high) that coupling may occur. Comparing Eqs. (3) and (4), this is seen to occur when

$$n_i(r) \approx \frac{a^2}{r^2} \frac{\bar{n}_i}{5.3} \tag{5}$$

Assuming a realistic compression ratio $r_{wall}/a \approx 2$, condition (5) can be stated thusly: The m = 0, k = 0 radial oscillation will couple to an Alfvén wave (outside the current channel) if the tenuous plasma density is roughly a twentieth of the average density in the core.

The rough scaling argument, presented above, may have consequences for rf heating schemes that use the m = 0, k = 0 radial mode. The m = 0, k = 0 geometry is particularly attractive because it requires no drive coils additional to the current transformers (I_ϕ or I_θ) themselves. Although the degree of coupling is an open question, it is possible that the magneto-acoustic wave could end up heating the tenuous plasma via the coupled Alfvén wave. (Strong kinetic damping of the Alfvén wave at low densities has been predicted theoretically.[13])

C. Experimental Observations on ZT-S

Figure 24 shows the toroidal magnetic fields versus time at six locations for shot 29183. The discharge is a stabilized pinch driven by a 55 kA toroidal current turned on at $t = 58.5$ μs and rising in 4.5 μs. After $t = 64$ μs the column thrashes violently, but for $61 \leq t \leq 64$ μs the plasma is well confined in a highly compressed state by the poloidal field.

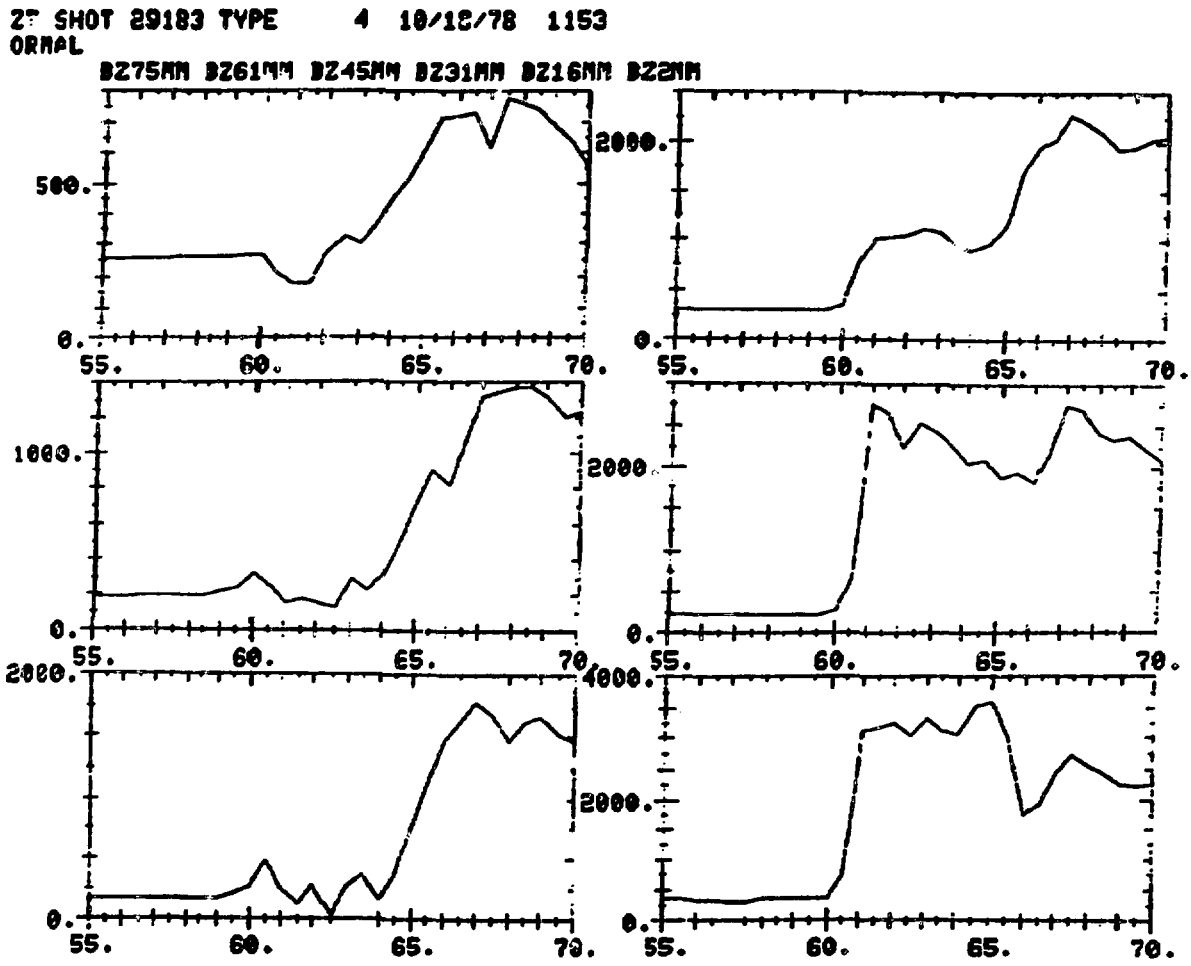

Fig. 24. Toroidal field versus time (during the dynamic phase of the pinch) at six internal locations for a stabilized pinch discharge (shot 29183). The radial positions in header are ordered top to bottom, with left column first and right column second.

The toroidal field near the axis shows little magneto-acoustic modulation. However, the trace at r = 4.5 mm shows large-scale modulation, with a period of 1.5 μs, during 60 μs ≤ t ≤ 64 μs. Figure 25 shows that this oscillation occurs immediately outside the plasma column. Figure 26, in which the field histories at the outer three locations are shown on an expanded scale, indicates that the 1.5 μs period oscillation is well localized near r = 4.5 cm. Figure 27 compares the toroidal fields at r = 4.5 cm and r = 0.2 cm. The oscillations are roughly in phase, so it is not likely that

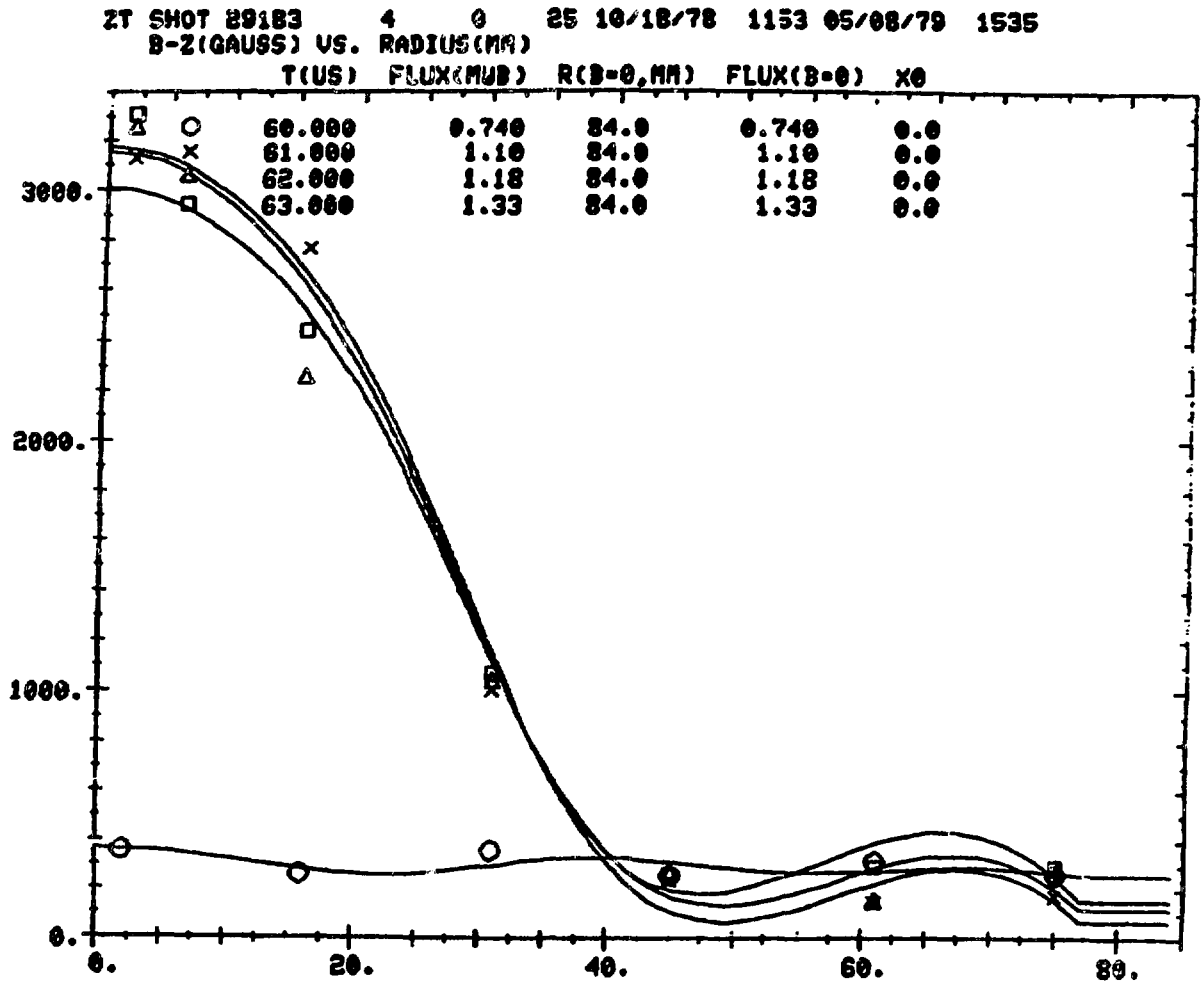

Fig. 25. Radial profiles of toroidal field at four times (separated by 1 μs) for a stabilized pinch discharge (shot 29183).

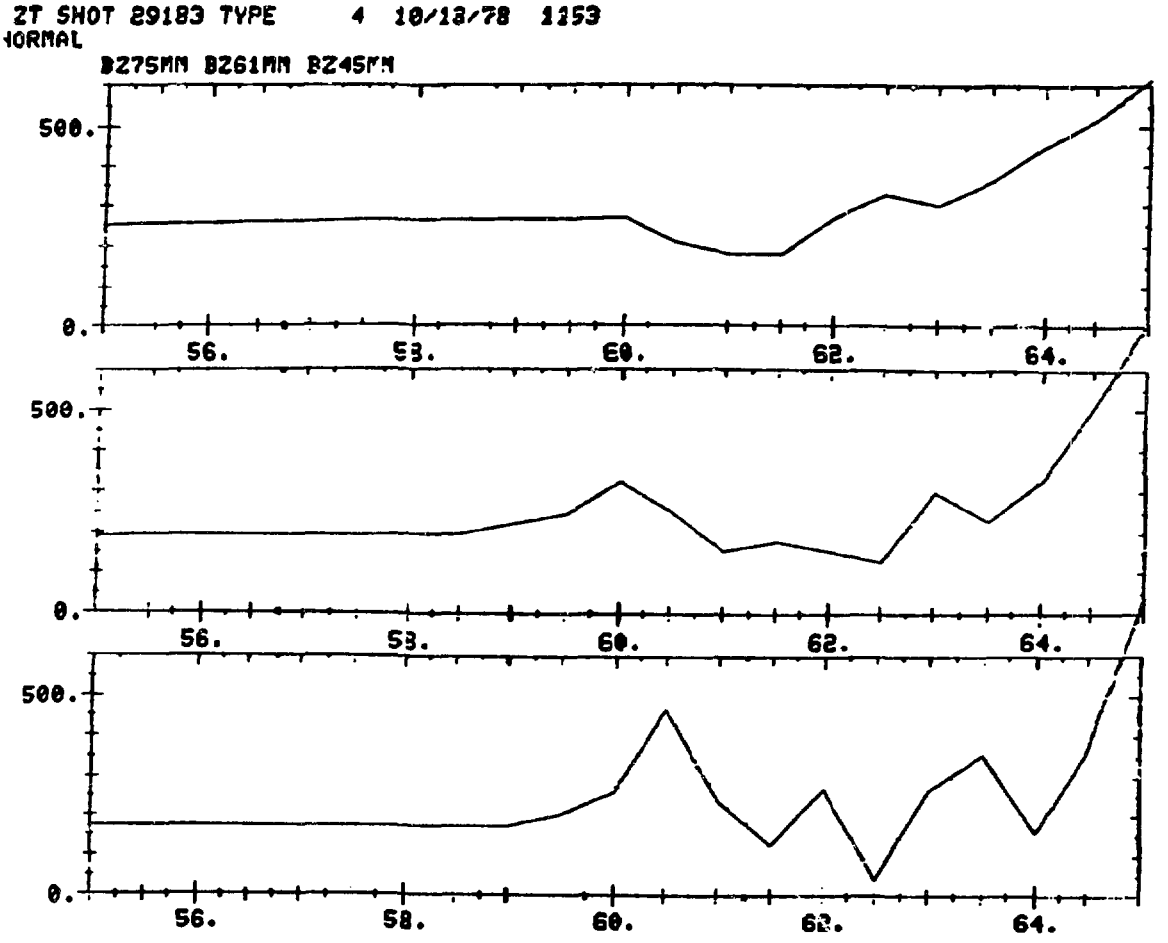

Fig. 26. Toroidal field versus time at 3 locations (order: top to bottom) for a stabilized pinch discharge (shot 29183). The probe at r = 45 mm shows a localized disturbance with period ≈ 1.5μs.

the activity at r = 4.5 cm is due to motion of the column boundary. (If it were, then the two traces in Fig. 4 would be modulated 180° out of phase.)

The Alfvén transit time expression [Eq. (1)] can be inverted to calculate the ion density required to support an Alfvén resonance at r = 4.5 cm. Using I = 55 ka, τ_A = 1.5 μs, and μ = 2 (deuterium),

$$n_i(4.5 \text{ cm}) \approx 0.4 \times 10^{15} \quad (\text{cm}^{-3})$$

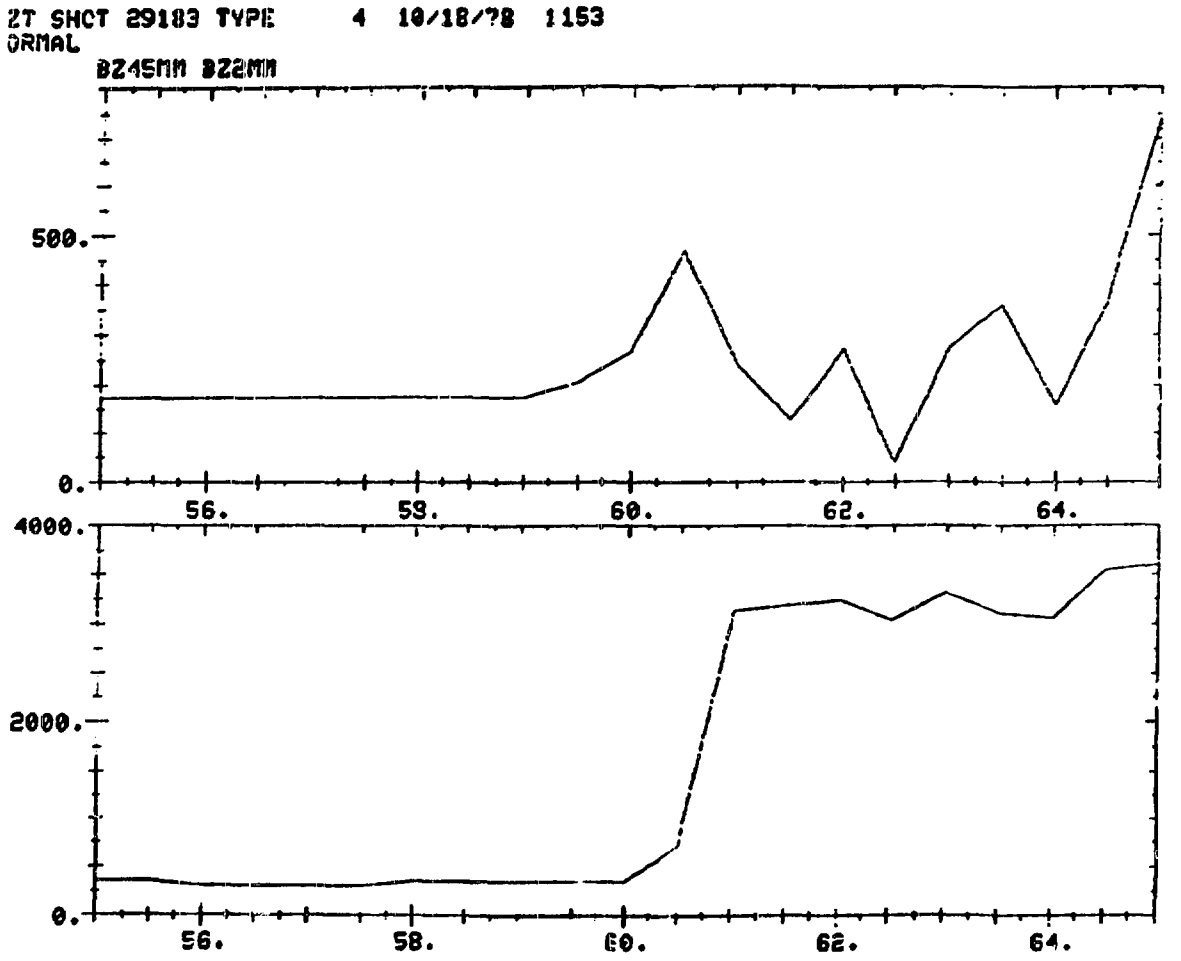

Fig. 27. Comparison of toroidal fields at oscillating surface (top) and near the axis (bottom) for shot 29183.

The data of Fig. 28 shows $\int n\, d\ell$ (double pass; $\lambda = 3.39$ μm) along a chord whose nearest approach to the axis is 5.1 cm. The <u>average</u> density along that chord, during 62 μs < t < 64.5 μs, is 0.2×10^{15} (cm^{-3}). Since the observed resonant location r = 4.5 cm lies slightly inside of this measurement chord, and since the density increases as the plasma core is approached, the inferred n_i is not inconsistent with interferometer data. The above argument suggests, though by no means proves, that the disturbance at r = 4.5 cm is an Alfvén wave caused by toroidal effects.

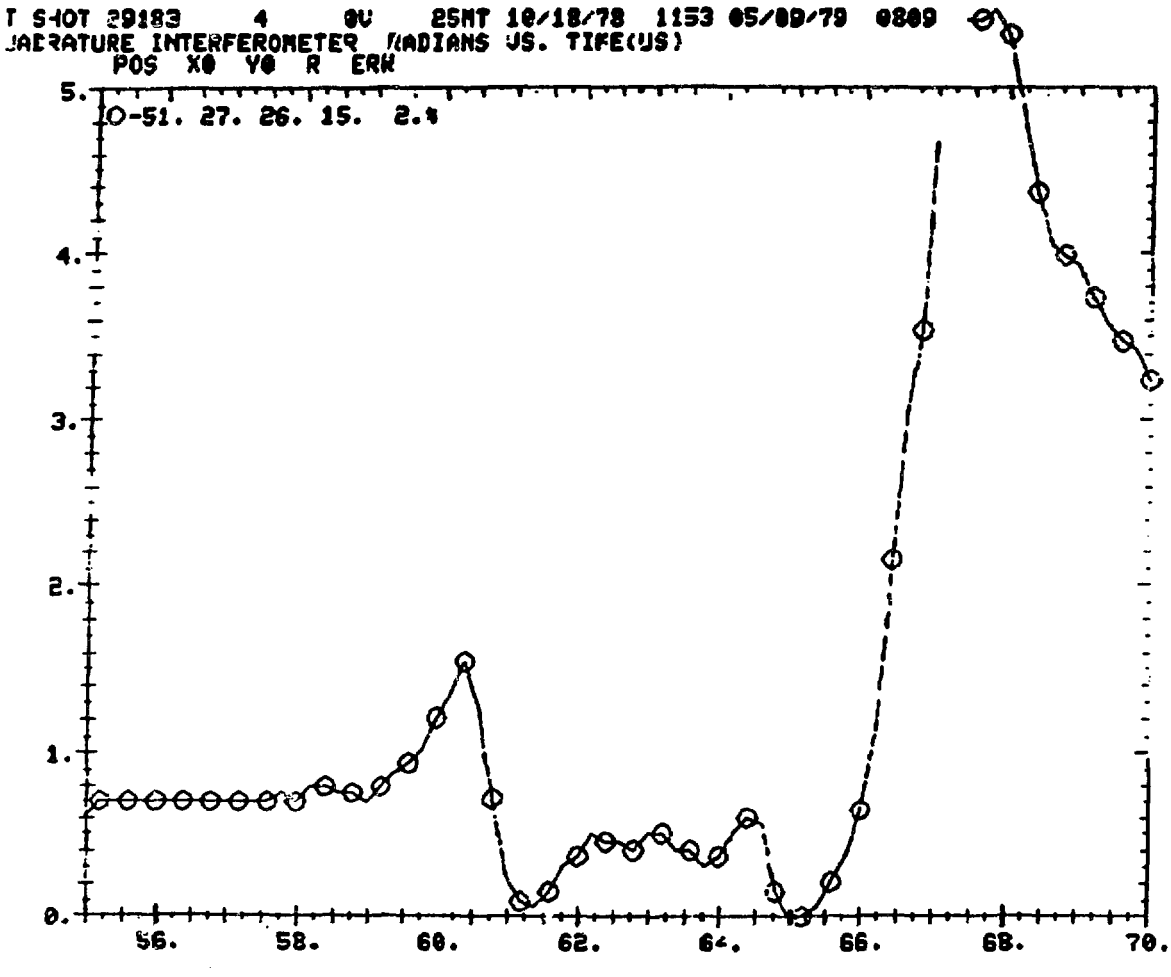

Fig. 28. Interferometer signal (radians; double pass) versus time for shot 29183, for the chord whose closest approach to axis is r = 5.1 cm. The abrupt rise at t = 66 μs is due to a violent instability.

Possible further evidence of such a shear Alfvén wave is provided by data from five consecutive discharges in the fast-rising I_ϕ mode (shots 28499-28503). The toroidal field histories (during the dynamic phase) at six internal locations are shown in Fig. 29. At the two innermost positions (middle and lower right) a strong magneto-acoustic oscillation is evident, with bounce period $\tau_B \approx 2.5$ μs. At t = 65 μs this motion becomes suddenly dampened. The toroidal field at r = 6.1 cm (middle left) shows an oscillation of the same period but which sharply increases in magnitude at t = 65 μs. (By

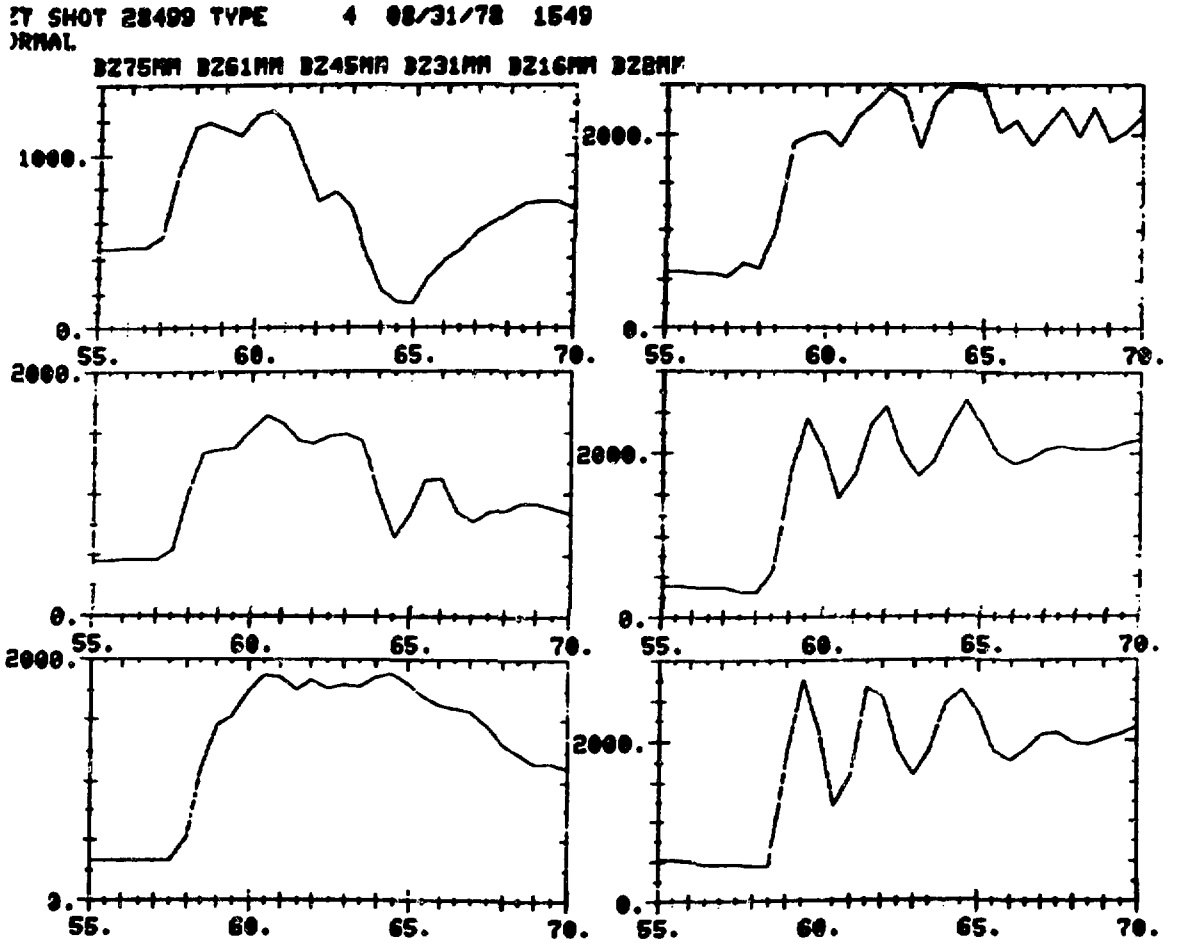

Fig. 29. Toroidal field versus time at six radii during dynamic phase of a pitch-programming discharge (shot 28499). (Times ordered as in Fig. 24.)

t = 65 μs, the external B_ϕ is ringing negative through zero.) The poloidal fields at six internal locations are shown in Fig. 30.

The sharp fluctuations of B_ϕ (at r = 6.1 cm) and B_θ (at r = 5.9 cm) are overlaid for five consecutive shots in Fig. 31. B_r, which is not measured, is expected to be small at this location due to image currents in the nearby conducting shell. The total field B_{total} can then be taken as $(B_\phi^2 + B_\theta^2)^{1/2}$ and is also shown in Fig. 31. From the fact that the fractional variations are much larger in B_θ and B_ϕ than in B_{total}, the oscillation is shear, as opposed to compressional.

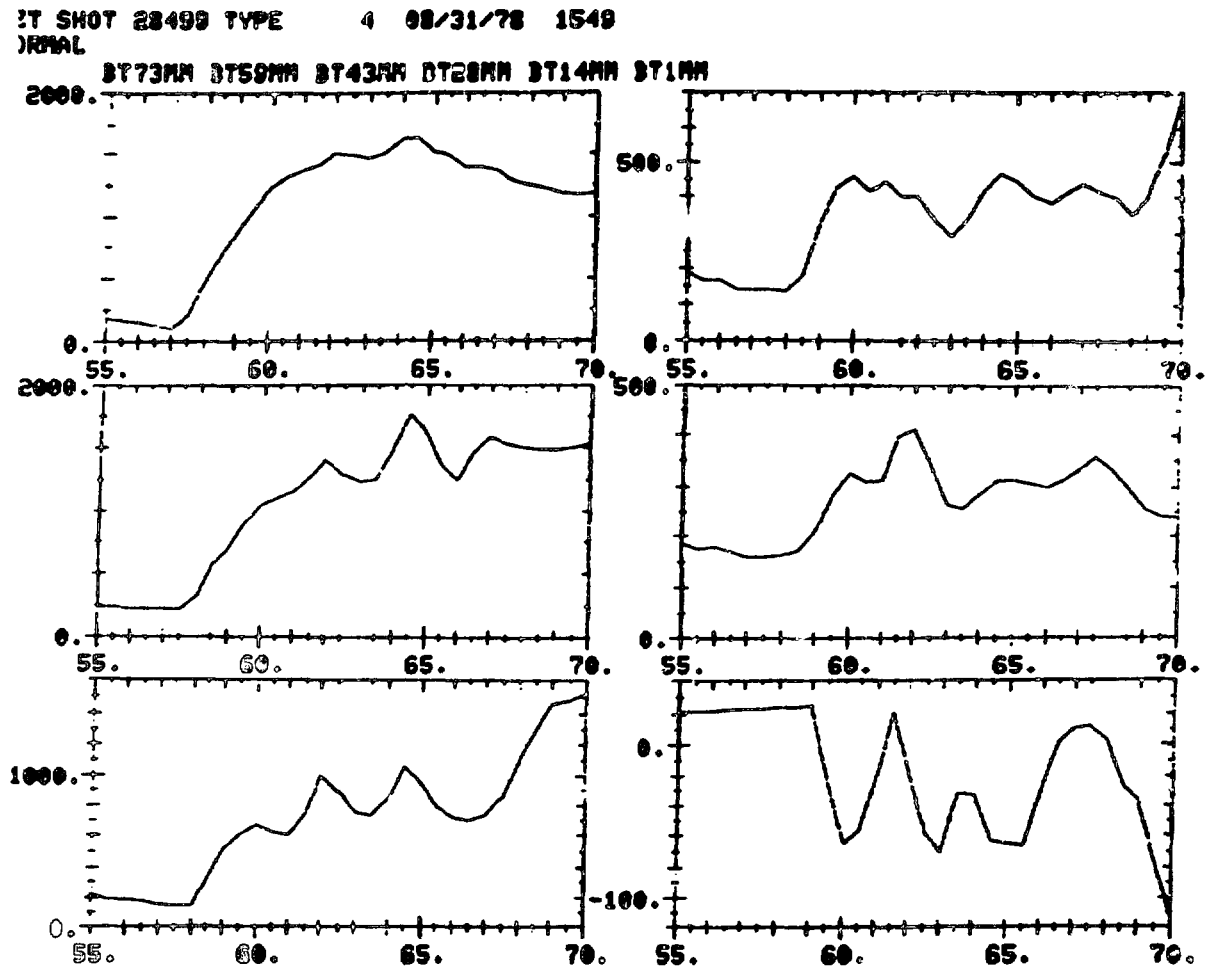

Fig. 30. Similar to Fig. 29, but poloidal field.

Assuming that $r \simeq 6$ cm is the site of an Alfvén resonance for $\tau_A = 2.5$ μs, the density can be inferred from Eq. (1), giving

$$n_i \simeq 0.23 \times 10^{15} \ (\mathrm{cm}^{-3})$$

at $r \simeq 6.0$ cm. This will be compared to interferometer data (as was done above for shot 29183). The phase shifts along five chords (double pass; $\lambda = 3.39$ μm) are shown in Fig. 32. The outermost chords (at

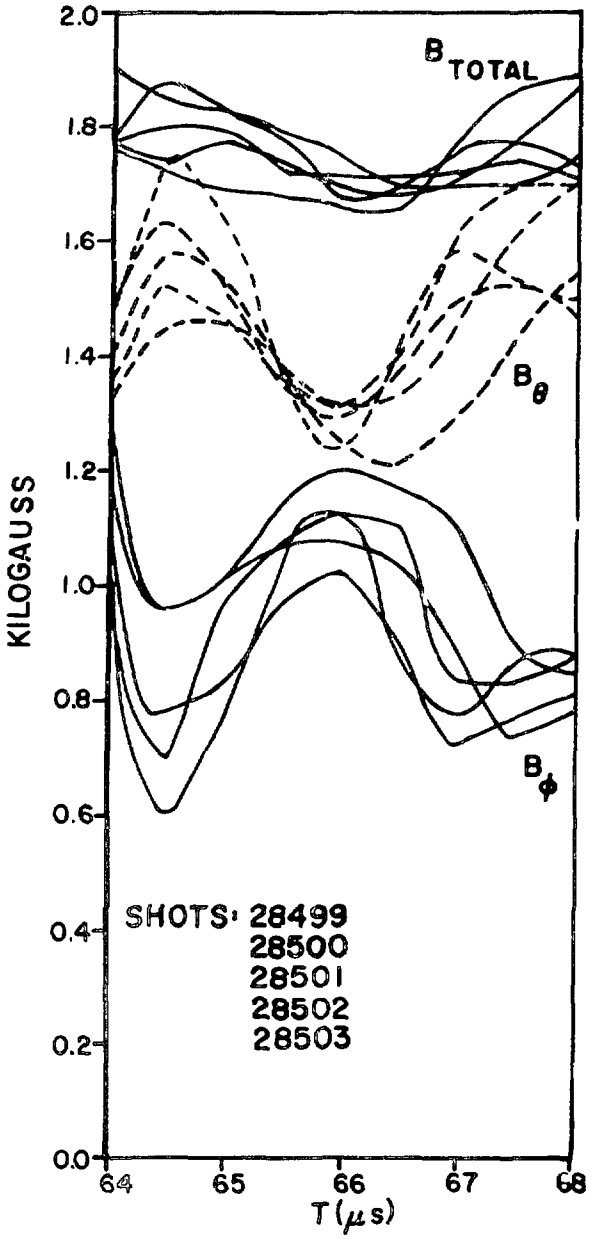

Fig. 31. Field components at r ≈ 6 cm for five consecutive pitch-programming discharges. The relative constancy of B_{total} compared to either B_θ or B_ϕ is evidence for a shear polarization to the disturbance. B_r, though not measured, is assumed negligible because of proximity to the conducting wall.

$R - R_o = \pm 5.1$ cm) pass closer to the plasma core than is the field measurement location (r ≈ 6 cm), so the measured average density along those chords (0.40×10^{15} cm^{-3}) at t = 65 μs probably represents an upper limit on the local density at r = 6 cm. Since this is larger (but still comparable to the inferred density, 0.23×10^{15} (cm^{-3}), at r = 6 cm, it is possible that the

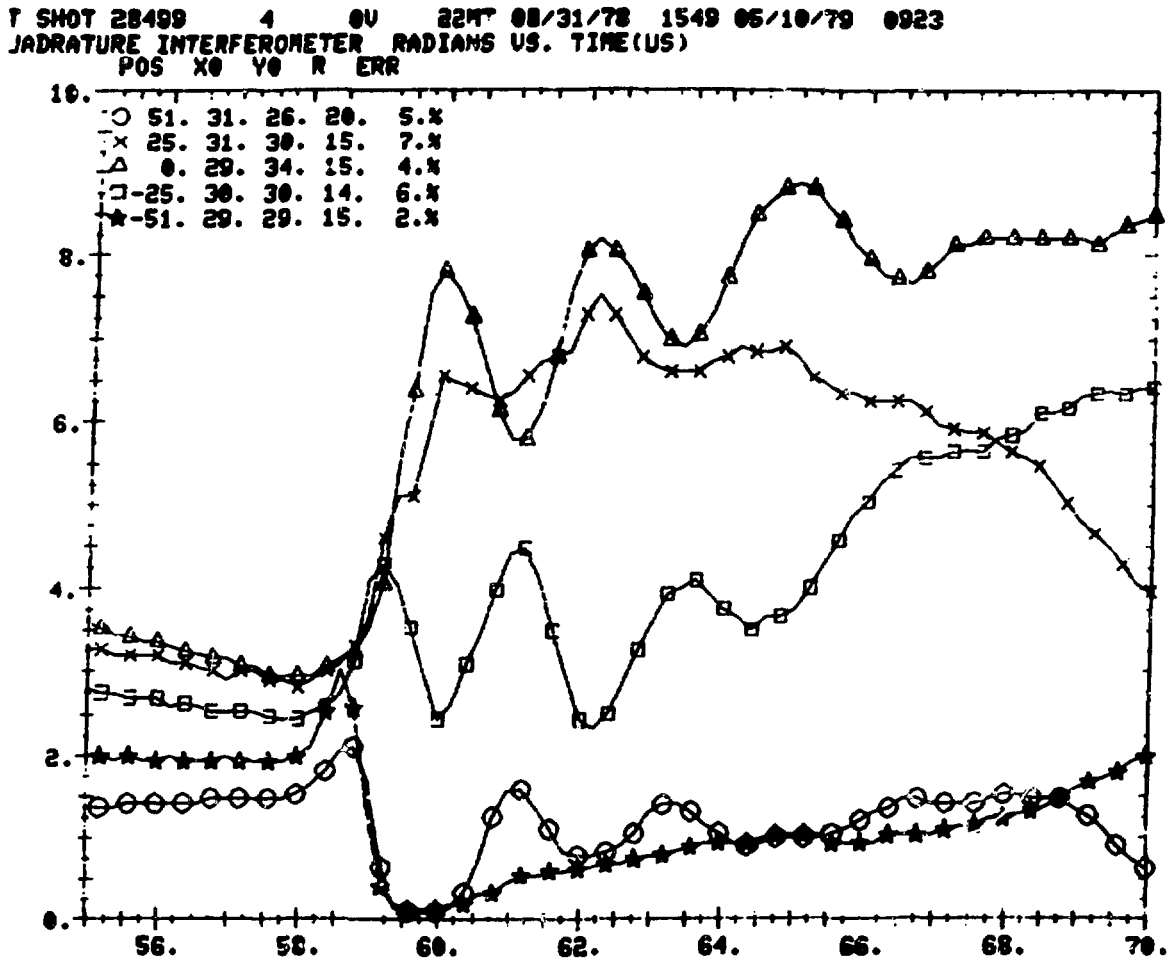

Fig. 32. Interferometer signals (radians, double pass) versus time along five chords during the dynamic phase of a pitch-programming discharge (shot 28499). The coalescence two chords (marked with crosses and squares) after t = 64 μs is due to a reduction in the outward toroidal shift.

magnetic field disturbance there is a manifestation of the Alfvén wave, driven by toroidal effects, described above. The presumed shear wave is at the same frequency as the magneto-acoustic oscillation which precedes it. Furthermore, the shear disturbance seems to be precipitated by the rapid interchange of toroidal with poloidal flux (in the outer third of the tube) which accompanies the programmed reversal of B_ϕ at the conductor. That interchange also causes a reduction in the outward toroidal shift (via the increase in internal inductance for the I_ϕ circuit). The latter effect is apparent from the

interferometer traces following t = 64 μs in Fig. 32. The change in toroidal shift may, in turn, initiate shear waves, with spatial periodicity equal to the pitch length, along the field lines.

ACKNOWLEDGEMENT

The entire on-line data acquisition and analysis software are due to Kenneth Klare.

REFERENCES

1. S. A. Colgate, J. P. Ferguson, and H. P. Furth, "External Conductivity Theory of Stabilized Pinch Formation," UCRL 5086 (1958).

2. C. Bobelddijk, R. J. J. van Heijningen, J. A. Hoekzema, P. C. T. van der Laan, D. Oepts, and A. A. M. Oomens, "Experimental Results of the Screw Pinch Experiment SPICA," Proceedings of 3rd International Conference on Plasma Physics and Controlled Nuclear Fusion, Tokyo (1974) Vol. III, p 409.

3. P. C. T. Van der Laan, personal communication Sept. 1977.

4. A. G. Sgro and P. C. T. Van der Laan, "Computer Modeling of Reversed-Field Pinch Formation," Bul. Amer. Phys. Soc., Vol 22, 9, p 1155 (Oct. 1977).

5. A. R. Jacobson, "Heterodyne Quadrature Interferometer for Simultaneous Measurements of Plasma Density Along Several Chords," Rev. Sci. Instrum. 49, (5) pp. 673-674 (May 1978).

6. Code supplied by Franz Jahoda, April 1979.

7. R. H. Huddlestone and S. Leonard, Plasma Diagnostic Techniques, Academic Press, N.Y.C. 1965.

8. Kenneth R. Lang, Astrophysical Formulae, Springer Verlay, N.Y.C. 1964.

9. A. Haberstich, 1969 CTR Annual Prog. Rept., Los Alamos Scientific Laboratory report LA-4351-MS, pp. 49-53, (1969).

10. A. J. L. Verhage, A. S. Furzer, D. C. Robinson, "Observations of Large-Amplitude Helical Kink Instabilities and Field Reversal in a Fast Pinch Experiment (HBTX-1)," Nucl. Fusion 18 4, pp. 457-473 (1978).

11. A. J. L. Verhage, A. S. Furzer, D. C. Robinson, "Observations of Large-Amplitude Helical Kink Instabilities and Field Reversal in a Fast Pinch Experiment (HBTX-1)," Nucl. Fusion 18 4, pp. 457-473 (1978).

12. J. A. Tataronis and W. Grossman, "On Supplementary Heating of Fusion Plasmas by Means of Alfvén Waves," Courant Institute Report COO-3077-102.

13. A. Hasegawa and Lui Chen, "Kinetic Process of Plasma Heating due to Alfvén Wave Excitation," Phys. Rev. Lett. 35, No. 6, pp. 370-373 (1975).